NASA TECHNICAL MEMORANDUM

NASA TM X-3467

NASA TM X-3467

APPARATUS FOR EXPERIMENTAL INVESTIGATION OF AERODYNAMIC RADIATION WITH ABSORPTION BY ABLATION PRODUCTS

William L. Wells and Walter L. Snow

Langley Research Center
Hampton, Va. 23665

NATIONAL AERONAUTICS AND SPACE ADMINISTRATION • WASHINGTON, D. C. • MARCH 1977

1. Report No.	2. Government Accession No.	3. Recipient's Catalog No.
NASA TM X-3467		

4. Title and Subtitle	5. Report Date
APPARATUS FOR EXPERIMENTAL INVESTIGATION OF AERODYNAMIC RADIATION WITH ABSORPTION BY ABLATION PRODUCTS	March 1977
	6. Performing Organization Code

7. Author(s)	8. Performing Organization Report No.
William L. Wells and Walter L. Snow	L-11168
	10. Work Unit No. 506-26-20-01

9. Performing Organization Name and Address	11. Contract or Grant No.
NASA Langley Research Center Hampton, VA 23665	
	13. Type of Report and Period Covered Technical Memorandum

12. Sponsoring Agency Name and Address	14. Sponsoring Agency Code
National Aeronautics and Space Administration Washington, DC 20546	

15. Supplementary Notes

16. Abstract

A description is given and calibration procedures are presented for an apparatus that is used to simulate aerodynamic radiant heating during planetary entry. The primary function of the apparatus is to simulate the spectral distribution of shock layer radiation and to determine absorption effects of simulated ablation products which are injected into the stagnation-region flow field. An electric arc heater is used to heat gas mixtures that represent the planetary atmospheres of interest. Spectral measurements are made with a vacuum ultraviolet scanning monochromator.

17. Key Words (Suggested by Author(s))	18. Distribution Statement
Ablation Radiant heating Electric arc heater Planetary entry Spectroscopy	Unclassified - Unlimited Subject Category 02

19. Security Classif. (of this report)	20. Security Classif. (of this page)	21. No. of Pages	22. Price*
Unclassified	Unclassified	45	$3.75

* For sale by the National Technical Information Service, Springfield, Virginia 22161

APPARATUS FOR EXPERIMENTAL INVESTIGATION OF AERODYNAMIC RADIATION WITH ABSORPTION BY ABLATION PRODUCTS

William L. Wells and Walter L. Snow
Langley Research Center

SUMMARY

Apparatus A of the Langley planetary entry radiation laboratory is used to experimentally investigate spectral radiation absorption by ablation products in the stagnation-region radiating flow field of an ablating blunt body during planetary entry. An ultraviolet scanning monochromator is used to measure the spectra from the radiating gas both with and without injection of simulated ablation products between the radiation source and the measuring instrument. Gas mixtures tailored to simulate the planetary atmospheres of interest are heated by passing them through an electric arc heater. Calibration by direct substitution of an arc source with known output intensity and determination of the efficiency of the optical components allow spectral measurements between wavelengths of about 100 nm and 850 nm.

An independent diagnostic optical system which utilizes a second spectrometer is used to determine the temperature of the arc-heated gas.

INTRODUCTION

Spacecraft entering the atmospheres of planets at high speed are subjected to severe aerodynamic heating which consists of all three forms of heat transfer - conduction, convection, and radiation. In cases where the entry velocity is very large, such as entry into the Jovian atmosphere, the radiation component becomes a major contribution to the heat load. Because of the importance of radiative heating to the design of heat protection systems for vehicles that make such entries, a great deal of analytical effort has been devoted to the study of this phenomenon. (For example, see refs. 1, 2, and 3.) Radiation phenomena are inherently very complicated and dependent upon a number of interrelated variables. Consequently, recent theoretical analyses have become very sophisticated and employ numerical techniques along with high-speed computers. (See refs. 4, 5, and 6.) However, a major uncertainty remains in knowledge of the interaction between radiation and ablation products because of a lack of experimental verification (ref. 7). Since the thermal protection system constitutes a high percentage of the total weight of a typical planetary probe, it is desirable to reduce the uncertainty in heat shield design so that valuable and costly vehicle space and weight can be devoted to the scientific payload. Consequently, it is desirable to simulate radiation phenomena in the laboratory where detailed measurements can be made to compare with theory.

In an actual entry, the radiative heat load is due to emission from the shock-heated gas and occurs over a broad band of wavelengths from vacuum ultra-

violet (VUV) through infrared (IR). The ablation concept seems to offer the best overall advantage for heat shields although heat storage and reflection system alternatives have been considered (ref. 8). In ablating systems, thermal decomposition of materials such as carbon phenolic causes gaseous ablation products to be injected into a flow field boundary layer where they often act as absorbers of the incident radiant flux. The extent of radiation blockage or absorption is dependent on a number of parameters, one of which is the wavelength, or frequency, of the radiation. For instance, gaseous carbon may absorb radiation in one wavelength range but be transparent in another range. (See refs. 9 and 10.) In certain circumstances, some ablation products may become significant emitters themselves and actually increase the radiant heat load in a particular wavelength range. Because of the complexity of the interrelated processes, simulation of these phenomena is difficult.

Simply stated, an experimental apparatus to simulate the radiation phenomena must

(1) Produce a very broad radiation spectrum (VUV through IR)

(2) Allow time for spectral measurements over this spectrum

(3) Allow injection of ablation products (simulated or real) between the measuring device and the emission source

Three devices were considered for the emission source: a shock tube, a laser, and an electric arc heater. The arc heater was selected because it can produce both a long run time and a broad emission spectrum tailored to the particular atmospheric gas in question. A special ablation gas injection system was designed, and a scanning monochromator and other optical components were obtained to complete the system.

A brief description of the system was given in reference 11; however, most of the emphasis there was on results and analysis. The present paper presents a more detailed description of the apparatus and calibration techniques. Only a few sample results are presented. The system described here is referred to as apparatus A of the Langley planetary entry radiation laboratory (PERL).

SYMBOLS

A	Einstein coefficient for spontaneous emission, s^{-1}-particle^{-1}
C	calibration factor, $V/(W/cm^2\text{-sr-nm})$
c	speed of light, 2.9979×10^{10} cm/s
D	diameter of aperture stop, cm
E	atomic energy level, cm^{-1}
e	photon energy, eV

G	geometry factor, cm^2-sr
g	degeneracy factor, dimensionless
h	Planck constant, 6.626×10^{-34} J-s
I	specific intensity, W/cm^2-sr
j	volume emission coefficient, W/cm^3-sr
k	Boltzmann's constant, 6.952×10^{-11} cm/K or 1.381×10^{-23} J/K
k_ν	extinction coefficient, cm^{-1}
N	total photon number when superscripted, s^{-1}; particle number density when subscripted, cm^{-3}
p	pressure, N/m^2
$p(\bar{\nu}),p(\bar{\lambda})$	fluorescent emission probability density, nm^{-1}
Q	quantum conversion efficiency of phosphor, dimensionless
$\dot{q}$	radiative heating rate, W/cm^2-s
R	maximum radius of cylindrical emitter, cm
r	radius, cm
S	source function, W/cm^2-sr
s	length, cm
s'	distance from source to imaging lens, cm
T	temperature, K
V	volume, cm^3
V_{sig}	signal voltage, V
w	optical parameter used to evaluate Abel inversion optics, dimensionless
x,y	Cartesian coordinates, cm
Z	partition function, dimensionless
β_{mn}	elements of Abel inversion matrix [β], dimensionless
$\beta_{\bar{\lambda}}$	photomultiplier responsivity, V/W

Δ zone width for Abel inversion, cm

ϵ component optical efficiency, dimensionless

λ wavelength, nm

ν frequency, s^{-1}

τ_λ spectral transmission, dimensionless

τ_ν optical depth, dimensionless

Subscripts:

E edge (outer) of ablation layer

e per unit energy

e^- electron

max maximum

R radiant

r reference; also reflected

t total

u upper

$u \to \ell$ upper to lower

W wall of blunt body

λ spectral

ν per unit frequency interval

Superscripts:

i in

o out

Abbreviations:

UV ultraviolet

VUV vacuum ultraviolet

Average over phosphor response is denoted by < >.

A bar over λ or ν denotes the wavelength or frequency of the radiation emmitted from a phosphor when it is bombarded by radiation of wavelength λ or frequency ν.

CONCEPT

Apparatus A of the Langley planetary entry radiation laboratory (PERL) was designed to experimentally investigate the various aspects of radiative heating which included the absorption of shock layer radiation by ablation products in the stagnation region of the flow field. The concept of the facility is shown in figure 1. A typical radiating shock layer is depicted for the stagnation region of a planetary probe, as well as the ablation layer which attenuates the radiant flux directed toward the body. In the simulation apparatus the test gas is heated by passing it through a wall-stabilized arc discharge. A cylindrical blunt body is located at the exit of the flow channel so that the gas is forced to turn and flow radially outward through a narrow gap into an evacuated chamber. The gap width is adjusted to provide the minimum flow area near the outer edge of the blunt body in order to assure subsonic flow in the central region. This arrangement produces a flow that roughly simulates the stagnation streamline of a blunt reentry body. A more detailed view is presented in the schematic of figure 2 in which the simulated ablation gas injector is also indicated. Radiation from the arc-heated gas travels through the injected ablation gas layer, through an aperture in the center of the blunt body face, and then through an optical system into the spectrometer. The spectrometer measurements can be made with and without simulated ablation gases, so that absorption effects can be determined. For baseline measurements without ablation gases, helium, which is transparent to the radiation, is injected through the injector ports. Detailed descriptions of the individual components are given in a subsequent section.

APPARATUS

Figure 3 presents a schematic diagram of the major components of the test apparatus. Photographs of the apparatus are shown in figure 4. Some of the major utilities such as power supply and cooling water system are shared by other test apparatus in the laboratory. A description of the major components of apparatus A is given in the following sections.

Arc Heater and Subsystems[1]

Arc heater.- In figure 5, a simplified view of the heater is drawn to scale with the blunt body and the primary optical system. The tubular flow channel of the wall-stabilized arc heater consists of a series of water-cooled annular copper disks, 0.95 cm thick, which are separated from each other by thin boron nitride insulators. The insulators, with an axial thickness of 0.21 cm, depend on heat conduction to adjacent copper disks for cooling. The insulators and the

[1]Barry N. Hogge provided special assistance in total systems integration and data acquisition.

cooled copper segments have a common inside diameter of 2.37 cm and, when assembled, form a flow channel 42 cm long. Immediately downstream and coaxial to the constant-diameter channel is a 14-cm-long section which increases in diameter to about 12 cm at the exit as indicated in figure 6. The test gas is heated by the arc which is struck from a hollow tungsten cathode at the upstream end to 32 water-cooled copper anode pins in the downstream expanded section. Each anode pin is individually connected to the power supply bus bar through a tungsten ribbon resistor located in the cooling water passage, so that the arc fans out and delivers a low-level current to each of the pins. A small quantity of argon is injected around each pin to provide a region of lower ionization potential and thereby reduce current density at the surface. When carbon dioxide is used as a test gas, the tungsten cathode is replaced by a graphite one. This was required because carbon dioxide dissociation liberated sufficient oxygen to cause rapid erosion of the tungsten cathode.

The heater is designed to operate at a maximum power of 1 MW or a maximum current of 1500 A.

Power supply and electrical circuit.- Direct current is supplied to the arc heater by a 6-MW power supply that consists of four modules which provide a nominal 1000 V each. Each module consists of a transformer and a silicon diode rectifier, and the maximum current capacity of each module is 1500 A. The modules can be operated individually or in any series or parallel arrangement desired. Most test gas mixtures require an open circuit voltage of 1000 V to ignite and maintain the arc, whereas mixtures with high hydrogen content require 2000 V because of the higher ionization potential of hydrogen.

The electrical circuit contains suitable switching and breaking equipment and a bank of resistors made of stainless steel tubes that are water cooled. The adjustable resistors provide resistive ballast for the arc and also provide current control. The circuit is not grounded so as to reduce the probability of current transfer to the blunt body at the arc heater exit during a test.

Test gas supply.- Test gases, in sufficient quantity to assure a constant flow rate throughout a test, are supplied to the arc heater from cylinders that are connected through manifolds. Systems for several gases are set up so that the atmosphere of the particular planet of interest can be simulated. The gases used are nitrogen or air (Earth); a mixture of nitrogen and carbon dioxide (Venus); and hydrogen, helium, or mixtures of hydrogen and helium (outer planets). Other gases could be used by changing fittings at the manifolds. The carbon dioxide piping includes a hot water heat exchanger to ensure the gaseous state of the carbon dioxide after it expands from the high-pressure storage cylinders and passes through the flow metering nozzle.

Ablation gas supply.- The ablation gas system is similar to the test gas system except that additional gases such as methane and carbon monoxide are supplied.

Vacuum system.- A vacuum system is used to exhaust all test and ablation gases from the facility. After the gases leave the test apparatus, they are ducted through a heat exchanger and from the system by one of two ways. For hydrogen or other gases that are considered fuels, a nitrogen-operated ejector

exhausts the gases into the atmosphere. For operation with all other gases, pumpdown vacuum spheres are used which provide a storage volume of about 292 m^3.

Cooling water system.- Cooling water is supplied by a pump at a pressure of 0.07 MN/m^2 from a large-volume (227 m^3) storage tank. The water is recirculated through a closed system.

Ablation Gas Injector and Blunt Body

Blunt body.- The blunt body is a 16.5-cm-diameter stainless steel cylinder that is open at one end and is closed at the other by a flat disk that is made of copper and is water cooled. The closed end faces the arc heater exit and has a 2.54-cm-diameter hole in the center where the ablation gas injector is positioned. This arrangement is shown in figure 7.

Injector.- The injector is made in three parts as shown in the sketch and photographs of figure 8. The front face is mounted flush with the front face of the blunt body. Three parallel walls form two chambers: one chamber receives the ablation gas and the other is evacuated. The two inner walls have a 1.52-mm-diameter hole at their centers which are coaxial with a 0.76-mm-diameter hole at the center of the outer wall. The outer wall also contains a pattern of 127 other 0.76-mm-diameter holes through which the ablation gases are injected into the main flow boundary. The evacuated chamber receives flow from the ablation gas chamber, as well as from the helium-purged optical system which is discussed subsequently. This differentially pumped arrangement allows a pressure in the ablation gas chamber that is independent of the optical system pressure. The center holes in the three walls are alined so as to pass the incident radiation into the optical tube. The front wall (face) is made of copper or carbon phenolic and depends on the simulated ablation gas for cooling.

Optical Systems

There are two optical systems: one is the primary system where the incident radiation and blockage effects are measured, and the second is a test gas diagnostic system.

Primary optical system.- The elements of the primary system are indicated schematically in figures 9 and 5. The first element is the 0.76-mm-diameter outer aperture in the injector face. A sealed 3.81-cm-diameter tube connects the injector to the spectrometer. Immediately behind the injector is a remotely operated ball valve which allows an unobstructed path for the radiation when open, but when closed seals off the remainder of the system while the injector or arc heater are open for maintenance. A calcium fluoride crystal window, 5.1 mm in diameter and 4.8 mm long, is located at the exit (spectrometer end) of the valve. The sealed window allows the spectrometer and optical tube to remain at a very low pressure throughout the test. To avoid transmission problems, the window is removed before measurements are made at wavelengths less than 200 nm. The next element is a limiting aperture that is 7.6 mm in diameter, and its function, along with the aperture in the injector face, is to define the cone of light entering the system both during a test and during calibration. This

arrangement also limits the field of view in the arc heater to the core region where the test gas temperature is nearly constant in the radial direction. The field of view encompasses a total plane angle of about 1.15° or a solid angle of 3.14×10^{-4} sr. The next element, a mirror, turns the incoming radiation through 90° and directs it onto the spectrometer entrance slit. The 5.08-cm-diameter mirror was formed by a platinum coating on the front surface of a spherically (67.3-cm-radius) concave pyrex blank. Because of off-axis astigmatism of the spherical mirror, the incoming circle of radiation falling on the mirror is projected as a vertical column on the narrow entrance slit of the spectrometer, which makes more efficient use of the radiation and therefore increases the sensitivity of the system. An order-sorting filter is located immediately in front of the spectrometer entrance slit. The filter can be inserted remotely, and its primary function is to cut off radiation of about one-half the wavelength of interest. Because of the diffraction characteristics of the spectrometer grating, wavelengths of higher orders can be projected into the exit slit if they are not filtered out.

Three different gratings are available. The gratings are described in table I along with a summary of the other optical component specifications. Selection of the proper grating and detector allows spectral measurements at wavelengths from about 100 nm to 850 nm. The final element in the system is the detector which is located behind the spectrometer exit slit. Two different photomultiplier tubes are available to be used as the detector; one has a spectral range from 165 nm to 680 nm, and the second from 165 nm to 850 nm. To extend the detection capability to lower wavelengths, a window coated with sodium salicylate phosphor is located in front of the photomultiplier tube. Such phosphor coatings have been used for a number of years and their properties are relatively well known. (See refs. 12 and 13.) At wavelengths below about 300 nm, virtually all the incident radiation is absorbed by the phosphor and is reemitted at wavelengths near 425 nm which can be detected by the tube. Therefore, radiation at wavelengths down to about 50 nm can be detected even though the tube itself has a higher cutoff at about 165 nm.

The spectrometer is a 1-m vacuum ultraviolet scanning monochromator and contains several of the optical elements discussed in the previous paragraphs. The optical chamber which contains the diffraction grating can be sealed and pumped to pressures as low as 3×10^{-6} torr (1 torr = 133.3 N/m^2) by use of an attached roughing pump and diffusion pump. External calibrated slit adjustment knobs are provided, the rate at which the spectrum is scanned can be varied, and the scan can be started or stopped or its direction (increasing or decreasing wavelength) controlled remotely. A tube with a valve is attached at the spectrometer end opposite the entrance and exit slits, through which ultrahigh-purity helium can be introduced into the system when measurements are made in the vacuum ultraviolet region of the spectrum. This will be discussed further in the section on procedures.

Diagnostic optical system.- The system used to spectroscopically determine the arc temperature is shown schematically in figure 10. A single apertured lens projects an undistorted image of the arc onto the entrance slit of a spectrometer. The arc is viewed in reflection off the front surface of the pivot mirror, which when rotated 90° allows an absolutely calibrated standard lamp to be viewed. Specially constructed viewing ports are placed where desired along

the arc axis. This is accomplished by replacing a standard arc channel segment with one that has been modified to contain a window-sealed slot as indicated in figure 11.

The spectrometer is a 1-m modified Czerny-Turner having an effective aperture of f/8.7. The instrument can be used in either a photoelectric or photographic mode. Using a 1200 groove/mm grating, the instrument has a wavelength range from 200 to 1300 nm with nominal resolution of 0.01 nm and a dispersion of 0.833 nm/mm. For the studies reported here the instrument was used in the photographic mode with 10.2-cm × 12.7-cm spectral analysis plates or Tri-X panchromatic cut film.[2]

The calibration system consisted of a 30-A tungsten strip filament enclosed in a special air-cooled housing and powered by a carefully regulated square wave electronic supply. The entire lamp system was calibrated by the Epply Laboratory, Inc. over the wavelength range from 250 to 2500 nm.

INSTRUMENTATION AND DATA SYSTEM

Instrumentation

The instruments associated with the optical systems have been described in the previous section. However, other instruments are used to make measurements to define the flow field and the radiating source. Measurements of pressure, wall heat flux, and voltage drop are made at several points along the length of the arc heater. The gas flow rates, arc current, and total voltage are also measured. These measurements, along with the diagnostic optical measurements, are used to verify theoretical arc-heated flow field calculations as in references 14 and 15. Pressure orifices are also located at nine radial points on the face of the blunt body. Pressures are measured with strain-gage transducers, cooling water temperatures with thermocouples, water flow rates with turbine flowmeters, gas flow rates with flow nozzles, arc current with a shunt, and voltages with saturable reactor transducers which are isolated from ground.

Data System

All data (except from the diagnostic optical system) are input to the data system as millivolt signals. The system will accept 45 analog channels of data which are sampled at a rate of 400 Hz with a range of $\pm$100 mV. The data are stored on magnetic tape during a test and are later converted and printed in engineering units or plotted on an x-y plotter.

---

[2]William C. Henley, Jr., provided special assistance in acquiring spectroscopic data.

OPTICAL SYSTEMS CALIBRATIONS

Primary System Calibration

A calibration factor C is obtained which relates the measured signal V_{sig} in V to the specific spectral intensity I_λ in W/cm^2-sr-nm and is defined by the relationship

$$V_{sig,\lambda} = C(\lambda)\, I_\lambda\, d\lambda \tag{1}$$

Above approximately 210 nm, C is obtained directly by recording the signal from a known radiance standard and using a modified substitution technique. The radiance standard in this case is the subliming anode of a low-current graphite arc. The characteristics of this source are well established and fully reported in references 16, 17, and 18. Since it is physically impossible to place the anode at the entrance aperture of the optical system, a modified substitution is used whereby the anode is one-to-one imaged by a single biconvex lens of known transmission onto the primary aperture. Care is taken to maintain and fill all apertures in the optical train as they would be under actual run conditions.

To measure UV radiation, a phosphor is used to up-convert the radiation into the visible regime. A convenient index for phosphors is the quantum conversion efficiency Q which is defined as

$$Q \equiv \frac{\text{Photons out}}{\text{Photons in}} \equiv \frac{N^o}{N^i}$$

The frequency of the emitted photon is governed by a probability density $p(\bar{\nu})$ which is characteristic of a particular phosphor. The relative probability curve for sodium salicylate is shown in figure 12. The number of photons emitted in the frequency range from $\bar{\nu}$ to $\bar{\nu} + d\bar{\nu}$ is accordingly $N^o\, p(\bar{\nu})\, d\bar{\nu}$. The radiant power conversion efficiency is obtained by multiplying by the energy per photon $h\nu$ at the stated frequencies, that is,

$$\text{Radiant power conversion efficiency} = \frac{N^o\, p(\bar{\nu})\, d\bar{\nu}\, h\bar{\nu}}{N^i h\nu} = \frac{Q\bar{\nu}\, p(\bar{\nu})\, d\bar{\nu}}{\nu} = \frac{Q\lambda\, p(\bar{\lambda})\, d\bar{\lambda}}{\bar{\lambda}}$$

where conversion to more convenient wavelength units has been accomplished by noting that probability is conserved ($p(\bar{\nu})\, d\bar{\nu} = p(\bar{\lambda})\, d\bar{\lambda}$). This up-converted radiant power is in turn converted to electrical power in accordance with the spectral responsivity of the photomultiplier $\beta_{\bar{\lambda}}$ in V/W. A typical S-11 response curve is also shown in figure 12. A flow chart relating the output signal to the incident radiant power is shown in figure 13.

The signal measured for photons converted into the wavelength range from $\bar{\lambda}$ to $\bar{\lambda} + d\bar{\lambda}$ is

$$dV_{sig,\lambda} = I_\lambda\, d\lambda\, G\tau_\lambda\varepsilon_\lambda Q \frac{\lambda}{\bar{\lambda}}\, p(\bar{\lambda})\, d\bar{\lambda}\, \beta_{\bar{\lambda}}$$

where specific spectral intensity I_λ is in W/cm^2-sr, geometry factor G in cm^2-sr, and photomultiplier responsivity $\beta_{\bar{\lambda}}$ is in V/W, so that the signal $V_{sig,\lambda}$ is in V. The detection system measures the entire output from the phosphor, so that

$$V_{sig,\lambda} = I_\lambda \, d\lambda \, G\tau_\lambda \varepsilon_\lambda Q\lambda \left\langle \frac{\beta_{\bar{\lambda}}}{\bar{\lambda}} \right\rangle$$

where $\langle\ \rangle$ denotes the average over the phosphor response $\left(\text{i.e.,} \left\langle \frac{\beta_{\bar{\lambda}}}{\bar{\lambda}} \right\rangle \equiv \int \left(\frac{\beta_{\bar{\lambda}}}{\bar{\lambda}} \right) p(\bar{\lambda}) \, d\bar{\lambda} \right)$. It should be clear from equation (1) that

$$C(\lambda) = \tau_\lambda \varepsilon_\lambda \lambda GQ \left\langle \frac{\beta_{\bar{\lambda}}}{\bar{\lambda}} \right\rangle$$

and if the spectral efficiencies and transmissions are known at some reference wavelength λ_r where the calibration factor has been measured directly, then

$$GQ \left\langle \frac{\beta_{\bar{\lambda}}}{\bar{\lambda}} \right\rangle = \frac{C(\lambda_r)}{\lambda_r \tau_{\lambda_r} \varepsilon_{\lambda_r}}$$

and

$$C(\lambda) = C(\lambda_r) \frac{\tau_\lambda \varepsilon_\lambda \lambda}{\tau_{\lambda_r} \varepsilon_{\lambda_r} \lambda_r} \qquad (\lambda \leq \lambda_r) \qquad (2)$$

A typical C curve is displayed in figure 14 and the procedure used to determine ε_λ is outlined in the appendix. In figure 14 the curve to the right of the vertical line was obtained directly from the graphite arc. The curve to the left of the vertical line was calculated from equation (2).

Diagnostic System Calibration

Temperature profile measurements using the diagnostic system have been based on absolute intensity methods and data were recorded photographically. Each calibration consists of a step exposure placed on the film in the darkroom prior to the test in order to establish the relative curve relating photographic density to exposure and also an absolute calibration using a certified standard lamp in the optical T-arrangement of figure 10. The absolute calibration exposure is recorded on site and subsequent to each successful facility run.

After ensuring that the radiation source has been imaged faithfully and with sufficient field depth, it is essential to have a stigmatic spectrograph which will reproduce the image at the film plane. This was verified in this case by imaging a reticle that was placed on the entrance slit through zero order and noting the lack of deterioration at the focal plane.

In addition, it is essential to guard against spurious reflections, since the interpretation of the measurements assumes that a given volume of emitting gas is viewed directly. To test for reflections from the back surface of the arc channel (refer to fig. 11(b)), a glowing Nichrome wire was placed coincident

with the channel center line and imaged through the system. Very little spurious scatter was observed. As a more practical test, the arc column was viewed directly with a variable exposure pyrometer camera (ref. 19). In the frames where the arc center line was overexposed, traces of reflection in the outer edges of the frames could be noted but were always weak and distinctly different in character from the desirable data.

TEST PROCEDURES

Supply voltage, ballast resistance, test and ablation gases, the spectrometer starting wavelength, and scan rate are all selected prior to a test. The gap between the arc heater exit and blunt body is adjusted to ensure subsonic flow upstream of the gap. The arc heater and region surrounding the blunt body are then evacuated to about 2 torr and cooling water flow is established. The following starting sequence is automated:

(1) A small amount of argon is injected into the arc heater through the test gas ports.

(2) Supply voltage is applied across the electrodes and the arc is ignited because of argon ionization.

(3) Test gas flow is established and the argon is shut off.

(4) Helium is injected through the ablation gas injector ports.

After stable operating conditions have been established, the optical tube valve (located behind the injector) is opened and a spectrometer scan of the desired spectral region is made while helium is flowing through the injector ports. A second scan is then made with the simulated ablation gas flowing instead of helium.

If the scan region of interest is in the VUV region, the evacuated spectrometer is flooded with high-purity helium (99.999 percent pure) so that the entire optical system is continuously purged when the optical tube valve is opened. Otherwise the system remains evacuated because of the seal at the calcium fluoride window.

Measurements made with the diagnostic spectrometer system are made independently of the other spectral measurements. The only requirement is that an equilibrium operating condition has been achieved within the arc heater before the shutter is operated to expose the film in the spectrometer.

DISCUSSION AND RESULTS

The measurement and interpretation of radiation data often involve assumptions and approximations. A clear statement of the general problem makes this evident. Three variables are of fundamental importance in radiation theory

(ref. 20). They are specific intensity I_ν (Radiant power/Projected area × Solid angle × Frequency interval), emission coefficient j_ν (Radiant power/Volume × Solid angle × Frequency interval), and extinction coefficient k_ν (Length^{-1}). If scattering is neglected, k_ν reduces to the absorption coefficient. The emission and extinction coefficients are not directly measured but must be inferred in conjunction with geometric considerations. It is convenient to define a differential optical depth $d\tau_\nu \equiv k_\nu\, ds$ where ds is a differential geometric path element, and also a source function $S_\nu \equiv j_\nu/k_\nu$. Then all problems of radiation involve solutions to the radiation transfer equation, namely,

$$\frac{dI_\nu}{d\tau_\nu} = S_\nu - I_\nu \tag{3}$$

with appropriate boundary conditions. The dependent variable is I_ν and the independent variable is the optical depth τ_ν; the source function is model dependent and for many laboratory plasmas can be reduced to the black body or Planck function to allow inference about the local temperature.

The solution for the homogeneous slab has a simple physical interpretation which is illustrated in sketch (a). In particular, if radiation is incident on

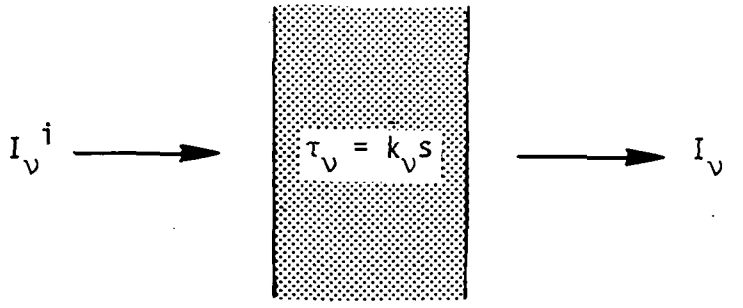

Sketch (a)

a lamina of radiating gas and is of magnitude $I_\nu^{\,i}$, then the solution contains an emission contribution and an exponential attenuation term as follows:

$$I_\nu = S_\nu(1 - e^{-\tau\nu}) + I_\nu^{\,i} e^{-\tau\nu} \tag{4}$$

Even fairly complicated sources can be considered to be made up of a succession of such slabs. Choice of apertures and calibrations can make this simple interpretation applicable.

Diagnostic System

The main purpose of the diagnostic system is to define the spatial temperature distribution in the source. The data are taken by exposure of photographic film to spectral radiation from a side view of the arc channel. Because of calibrations, the density of the exposed film can be related to the incident intensity; however, it is the radiating species number density which, through equilibrium composition tables, can be related to temperature. This procedure is

briefly discussed here and the reader is referred to reference 21 for details of the derivation and practical applications.

The diagnostic equipment samples spatial averages over regions of widely varying emission since the arc is viewed from the side (figs. 10 and 11(b)). Removing or "inverting" the geometrical weighting factors can be done under limited circumstances. Usually some region of the spectrum can be found which is "optically thin" which in equation (4) means to neglect absorption and assume that τ_ν is small enough so that $e^{-\tau_\nu} \equiv 1 - \tau_\nu$. In this case I_ν, the observable, is directly related to j_ν and the incident intensity. Physically, the thin condition assumes that the detected photons faithfully reflect the number of active atoms in the originating volume element.

Because of the cylindrical symmetry of the arc (see sketch (b)), it can be assumed that the emission coefficient j_ν depends solely on r, the radial

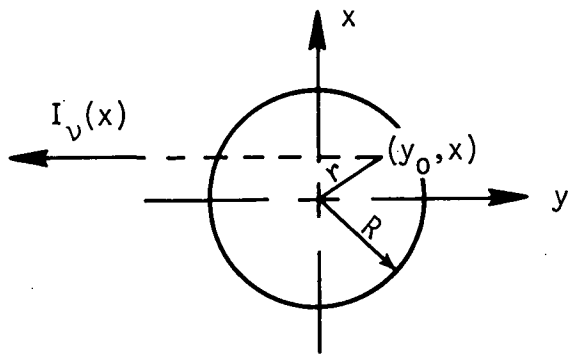

Sketch (b)

coordinate of the volume element in the source. Then with the coordinate choice depicted in sketch (b), it can be shown that

$$I_\nu(x) = 2\int_{y=0}^{y=y_o} j_\nu(r)\, dy = 2\int_{r=x}^{r=R} \frac{j_\nu(r)\, r\, dr}{(r^2 - x^2)^{1/2}} \tag{5}$$

which is an Abel integral form. The solution to this equation can be written as

$$j_\nu(r) = \frac{1}{2\pi r}\frac{d}{dr}\left[2\int_{x=r}^{x=R} \frac{I_\nu(x)}{(x^2 - r^2)^{1/2}}\, x\, dx\right] \tag{6}$$

where R is the radius of the arc column beyond which emission is negligible.

For engineering applications, equation (6) is not very useful since $I_\nu(x)$ is not known analytically. It is convenient to represent $I_\nu(x)$ as a data vector evaluated at equispaced intervals of x; that is, the cylinder is considered to be broken up into thin isothermal concentric annular zones of width Δ as indicated in figure 15. Then the nth component of $I_\nu(x)$ is $I_\nu(n\Delta)$ where

$n = 0, 1, \ldots, N$ and N is the number of annular zones. This approximation necessarily quantizes $j_\nu(r)$ with $j_\nu(m\Delta)$ representing the average emission coefficient of the mth annular region. These considerations reduce the integral equation to a set of simultaneous equations which can be solved by matrix methods. A number of alternative approaches have been suggested and Barr's formulation (ref. 22) is used exclusively in this work since it incorporates a certain amount of smoothing. Barr's matrix $[\beta]$ is devised so that

$$j_\nu(m\Delta) = \frac{1}{\pi\Delta} \sum_{n=0}^{N} \beta_{mn} I_\nu(n\Delta) \tag{7}$$

Under optically thin conditions, spectroscopic techniques determine the number densities of the species responsible for the emission. For a given gas with known pressure and in local thermodynamic equilibrium, the number density is a function of temperature only. As an example, if N_u is the excited state number density and $A_{u\to\ell}$ the transition probability per second for the transition, then

$$j_\nu = \frac{1}{4\pi} N_u A_{u\to\ell} h\nu \tag{8}$$

which is in W/cm^3-sr, and

$$N_u = \frac{N_t(p;T)}{Z(p;T)} g_u e^{-E_u/kT} \tag{9}$$

where N_t is the total number density, g_u is the degeneracy of the upper state having energy E_u, k is Boltzmann's constant, and Z is the partition function. Once N_u is determined from a measure of the emission coefficient and knowledge of atomic constants, the temperature consistent with this value is inferred from equation (9) and composition tables for a specified pressure. When two temperatures are consistent with the measurement, it is usually possible to rule out one of them on physical grounds or with the measurement of another property. As an example, in figure 16 the common upper state number density for two nitrogen lines of wavelength 493.5 and 491.5 nm is plotted as a function of temperature along with the electron density N_e-. Two temperatures are consistant with a single value of N_u, but note that as that curve decreases the N_e- curve increases. The free-free continuum intensity which depends on electron density squared would become a viable alternative for temperature determination above 13 000 K.

A typical radial temperature profile inferred for the arc using the diagnostic system is shown in figure 17. The test gas is nitrogen at a pressure of 0.5 atm (1 atm = 0.101 MN/m^2) and the arc current is 1000 A. The two nitrogen lines previously mentioned give nearly identical results. The viewing window was located at about one-half the arc channel length. Another example is shown in figure 18 where several measurements were made at different locations along the arc channel in a comparable sister facility (apparatus B). The emission coefficient is indicated instead of temperature and it is for 1 nm of continuum centered at a wavelength of 495.5 nm. For this case the test gas was nitrogen at a pressure of 0.5 atm but with an arc current of 540 A. Under these lower current conditions and in conjunction with the gas flow rate, the arc apparently

does not fill the channel. Monitoring the axial electron density (continuum source) in this manner is useful in assessing theoretical arc programs and for interpretation of spectra taken with the primary spectrometer which views the arc axially.

There are several sources for error in determining the temperature with this system. These sources and the estimated error they produce are line shape effect (see ref. 21), 2 to 3 percent; apertures, 2 to 3 percent; filters, 1 percent; calibration radiance, 3 percent; and inability to fit the experiment exactly to the Abel case, about 4 percent. The estimates were made on the basis of an analysis of variance scheme outlined in reference 23 which results in an overall 5 percent variance in the emission coefficient estimate. The transition probabilities for the nitrogen lines previously discussed have approximately 10 percent accuracy (ref. 24), so the error in the inference of N_u should be 10 to 12 percent. However, because of the exponential dependence on temperature, this entails only a few percent inaccuracy in temperature measurements at the arc center line.

Efforts made to reduce error due to the fit of experiment to the Abel case are probably worthy of a brief discussion. The interpretation in terms of Abel's integral equation is justified only to the extent that the system collects parallel pencils of light along chords in the source. Practically, this can only be approximated by imaging the source onto the spectrograph slit with a single lens, L, which is stopped down by an aperture of diameter D. (Refer again to fig. 15.) The collected pencils are slightly converging and underestimate the actual volume element in the source from which the emission derives. In reference 21 the relative volume error is derived from geometric considerations to be

$$\frac{\Delta V}{V} \leq 1 + \frac{2}{\pi}\left[\cos^{-1}\left(\frac{1 + w}{2}\right) - \cos^{-1}\left(\frac{1 - w}{2}\right)\right] + \frac{1}{2\pi}\left[(1 - w)\sqrt{(3 - w)(1 + w)}\right.$$

$$\left. - (1 + w)\sqrt{(3 + w)(1 - w)}\right] \qquad (10)$$

Where the parameter $w = (1 - RD/s'\Delta)/(1 + R/s')$ should be as close to 1 (the Abel case) as practical. For $w = 0.95$ the error is on the order of 3 to 4 percent. The ratio R/s' must be large and the aperture stop diameter D must not be too much larger than the zone spacing since it would compromise the ratio. The ratio s'/D is also involved in establishing the depth of field and must be large enough so that each point in the source is in crisp focus; otherwise, the volume elements would not be weighted equally, contrary to the implicit assumption in the derivation of the Abel equation. For a typical test in this work, $R/s' = 12.7$ mm/508.0 mm and $D/\Delta = 1.6$ mm/1.0 mm for a w of 0.94.

Primary Experiment

It is convenient to consider the experiment in terms of three distinct regions:

(1) The radiant source

(2) The primary optical system

(3) The injector

These three regions are discussed sequentially in the following paragraphs.

Radiant source.- The radiant source is the test gas which is heated by the electric arc to a temperature on the order of 15 000 K at the tube center line. The temperature is largely a function of the gas and the power input. Test gases that have been used to date in this apparatus are nitrogen, carbon dioxide, hydrogen, helium, and mixtures of hydrogen and helium. The radial and axial temperature profiles are determined both by the diagnostic optical system experimentally and by use of theoretical computations carried out with computer programs like the one in reference 25. Experimental measurements have also been made of axial gradients in pressure, voltage, and wall heat flux. These parameters have been computed for some cases where the thermodynamic and transport properties were available for these high-temperature conditions. Good agreement is obtained between experiment and theory for most parameters, as indicated in reference 14. A detailed knowledge of the radiant source is desirable so that the spectral radiation intensity incident on the injector surface (optical system entrance aperture) can be computed and compared with measurements. A detailed spectral radiation computer code is available (ref. 26) and is similar to that used in calculating radiating flow fields of outer planet entry (ref. 27).

The heater electrode design allows fixed arc attachment points and consequently a very steady arc is evidenced by observation of the glowing exit flow and by constant values of arc current and voltage. This desirable feature assures a constant radiant source as it is scanned across the wavelength interval of interest.

Primary optical system.- It was found necessary to keep the valve at the entrance of the optical tube (immediately behind the injector) closed until after the arc heater was started. Apparently, upon arc ignition a sufficiently high-pressure pulse is generated to drive contaminants off the arc heater surfaces and into the optical system. After repeated tests, this results in a gradual fogging of the platinum mirror in the case of VUV operation or fogging of the calcium fluoride window for tests at other wavelengths. When VUV measurements are being made, the system must be continually flooded with ultrahigh-purity helium (99.999 percent pure). Even though stock helium has a purity listed as 99.995 percent, apparently minute amounts of oxygen present throughout the long path length are sufficient to absorb the VUV radiation. The total path length consists of approximately 2.6 m external and 2 m internal to the spectrometer. Use of a liquid nitrogen cold trap and an activated charcoal desiccant for removal of moisture from the stock helium did not resolve the problem.

Injector.- The front surface of the injector is protected against melting by the flow of injected gas through numerous small holes in the face. The injector face has been made of either copper or carbon phenolic. The copper face is 0.152 cm thick and the carbon phenolic face is 0.635 cm thick. The carbon phe-

nolic surface temperature can be allowed to rise to a much higher value then copper, and the thicker face allows the injected gas to rise to a higher temperature also. This more nearly simulates the thermal environment of an entry probe ablating surface. The relatively cool copper ($T_{melt} \approx 1355$ K) removes the possibility of ablation products that could absorb incident radiation during the time when the reference spectrum is being measured. When a new injector face is installed, a new calibration of the optical system is required.

Example of experimental results.- To compare measurements with radiative transfer calculations, specific intensity per unit wavelength I_λ is related to specific intensity per unit energy I_e by

$$I_e \, de = I_\lambda \, d\lambda$$

or

$$I_e = -I_\lambda \frac{d\lambda}{de} = I_\lambda \frac{\lambda^2}{hc} \tag{11}$$

since

$$\lambda = \frac{hc}{e}$$

An example of results obtained in the Langley planetary entry radiation laboratory (PERL) is shown in figure 19. Shown in this figure is the measured intensity per unit energy as a function of energy in electron volts where the test gas is nitrogen, the arc current is 1000 A, and the pressure in the arc is 0.5 atm. In figure 19(a) the measured spectrum is shown for which helium was injected through the ablation gas injector. Since helium is transparent to the radiation, this is considered the "reference" or "no ablation" case. The continuum portion of the spectrum as computed with reference 26 is also shown for the no ablation case. Notice particularly the structure at 10 to 12 ev (λ from approximately 120 nm to 100 nm). In figure 19(b), nitrogen has been injected instead of helium, and the spectrum has been scanned again. There is some difference in the spectra of figures 19(a) and 19(b), but the basic structure is unchanged. However, when methane (CH_4) is the injected gas, as shown in figure 19(c), the radiation between 9 and 12 ev is almost completely eliminated. This represents a significant reduction in the total heat load and results from absorption of radiation by carbon and hydrogen which are primary constituents of actual ablation products. This example illustrates the concept of the planetary entry radiation laboratory. Further analysis will relate measurements to theoretical computations and thereby provide insight as to the credibility of existing radiating-absorbing flow field theories.

CONCLUDING REMARKS

A description of apparatus A of the Langley planetary entry radiation laboratory has been given along with calibration techniques employed. The radiation spectra for entries into atmospheres of various planets can be simulated by heating appropriate gas mixtures with an electric arc heater. A specially designed

injector allows injection of simulated ablation gases between the radiating source and a scanning vacuum ultraviolet monochromator. One sample case indicates that certain simulated ablation gases can greatly reduce portions of the radiation intensity spectrum.

A second spectrometer is used along with an Abel inversion technique to determine the temperature profile of the radiating gas when the gas can be considered optically thin.

Langley Research Center
National Aeronautics and Space Administration
Hampton, VA 23665
January 18, 1977

APPENDIX

DETERMINATION OF SPECTRAL OPTICAL EFFICIENCY ε_λ

In order to determine the optical efficiency of a mirror or grating, a special reflectance chamber coupled with a 0.5-m spectrometer and VUV light source was utilized. The light source provides the radiation over the wavelength interval of interest. The spectrometer disperses the light and projects the desired monochromatic beam into the reflectance chamber where it is measured. This apparatus is shown schematically in figure 20. The reflectance chamber contains a mounting stand for the mirror or grating and a sodium-salicylate-coated photomultiplier tube which may be located in one of two positions by use of an external knob. In the first position the photomultiplier receives the monochromatic beam directly from the monochromator, and in the second position it receives the reflected beam from the optical element in question. (Refer to fig. 20.) The spectral optical efficiency is defined here then, as the ratio of the detector signal $V_{sig,r}$ resulting from the diffracted or reflected beam to the signal $V_{sig,i}$ resulting from the direct beam at a specified wavelength, that is,

$$\varepsilon_\lambda = \left.\frac{V_{sig,r}}{V_{sig,i}}\right|_\lambda$$

The mounting stand can be rotated about its vertical center line by use of an external knob which is graduated in degrees. A window or filter inserter is located near the entrance of the reflectance chamber for order sorting of the incident light from the spectrometer grating. All controls are external to the system since VUV measurements are made while the system is evacuated. The VUV light source is a capillary gas discharge lamp which is described in reference 28. For measurements at higher wavelengths other sources such as a xenon lamp may be used.

The procedure to obtain the optical efficiency is as follows. After the system has been evacuated and the light source has reached a stable operating condition, the spectrometer is set to project light of the desired wavelength into the reflectance chamber. The chamber is closed so that no light enters it and the photomultiplier dark noise is "zeroed" out of the measuring circuit. The chamber entrance is then opened and the monochromatic beam is allowed to fall directly on the detector, at which time the output signal meter is adjusted to read 100 percent. After again checking zero, the detector is then rotated to the second position where the reflected beam is intercepted. In this position the output meter then reads the percent efficiency directly. The actual output signal is always monitored so that slit adjustments can be made to control the light input and thus avoid saturation of the photomultiplier tube. After the readings are recorded, the spectrometer is advanced to the next wavelength of interest and the sequence is repeated.

Diffracted light of the first order is measured during the experiment; consequently it is light of the first order that is of interest when the efficiency is determined. Efficiency in the zero order or second order may also be deter-

mined however, by rotation of the grating through the required angle. A typical set of efficiency curves for the 600 grooves/mm grating and a platinum-coated concave mirror is shown in figure 21. The grating efficiency curve is for first order light. Note that in the windowless mode of operation, second order light (of about 90-nm wavelength) begins to affect the shape of the curve at about 180 nm, and therefore filtering is required to exclude this indeterminate amount of lower wavelength light. Data affected by inclusion of second order light are ignored in the final construction of the curve. Two different light sources were used to obtain the data: a capillary hydrogen discharge lamp which operated at a pressure of 1 torr and a quartz-enclosed xenon lamp. The system was at a pressure of 1 atm when the xenon lamp was used and at 5×10^{-5} torr for the capillary discharge lamp. Differential pumping was required between the discharge lamp and the rest of the system, since there is no window on the lamp.

REFERENCES

1. Howe, John T.; and Viegas, John R.: Solutions of the Ionized Radiating Shock Layer, Including Reabsorption and Foreign Species Effects, and Stagnation Region Heat Transfer. NASA TR R-159,1963.

2. Olstad, Walter B.: Blunt-Body Stagnation-Region Flow With Nongray Radiation Heat Transfer - A Singular Perturbation Solution. NASA TR R-295, 1968.

3. Anderson, John D., Jr.: An Engineering Survey of Radiating Shock Layers. AIAA J., vol. 7, no. 9, Sept. 1969, pp. 1665-1675.

4. Garrett, L. Bernard; Smith, G. Louis; and Perkins, John N.: An Implicit Finite-Difference Solution to the Viscous Shock Layer, Including the Effects of Radiation and Strong Blowing. NASA TR R-388, 1972.

5. Moss, James N.: Stagnation and Downstream Viscous Shock-Layer Solutions With Radiation and Coupled Ablation Injection. AIAA Paper No. 74-73, Jan.-Feb. 1974.

6. Sutton, Kenneth: Coupled Nongray Radiating Flow About Ablating Planetary Entry Bodies. AIAA J., vol. 12, no. 8, Aug. 1974, pp. 1099-1105.

7. Congdon, W.: Major Uncertainties Influencing Entry Probe Heat Shield Design. Proceedings Outer Planet Probe Technology Workshop, NASA CR-137543, 1974, pp. VI-27 - VI-36.

8. Nicolet, W. E.; Howe, J. T.; and Mezines, S. A.: Outer Planet Probe Entry Thermal Protection: Part II: Heat-Shielding Requirements. AIAA Paper No. 74-701, July 1974.

9. Nelson, H. F.: Radiative Transfer Through Carbon Ablation Layers. J. Quant. Spectry. & Radiat. Transfer, vol. 13, no. 5, May 1973, pp. 427-445.

10. Moss, James N.; Anderson, E. Clay; and Bolz, Charles W., Jr.: Viscous-Shock-Layer Solutions With Radiation and Ablation Injection for Jovian Entry. AIAA Paper No. 75-671, May 1975.

11. Walberg, G. D.; Wells, W. L.; Houghton, W. M.; and Midden, R. E.: PERF: A New Approach to the Experimental Study of Radiative Aerodynamic Heating and Radiative Blockage by Ablation Products. AIAA Paper No. 74-1272, Oct. 1974.

12. Samson, James A. R.: Techniques of Vacuum Ultraviolet Spectroscopy. John Wiley & Sons, Inc., c.1967.

13. Zaidel', A. N.; and Shreider, E. Ya. (Z. Lerman, transl.): Vacuum Ultraviolet Spectroscopy. Ann Arbor-Humphrey Sci. Pub., 1970.

14. Wells, William Lee: Experimental Investigation of a Wall Stabilized Arc With Comparisons to Theoretical Predictions. M.S. Thesis, George Washington Univ., June 1973.

15. Walberg, Gerald David: Analysis of a Wall-Stabilized-Arc Discharge With Three-Dimensional, Non-Grey Radiation Transport. Ph. D. Thesis, North Carolina State Univ. at Raleigh, 1974.

16. Hattenburg, Albert T.: Spectral Radiance of a Low Current Graphite Arc. Appl. Opt., vol. 6, no. 1, Jan. 1967, pp. 95-100.

17. Pitz, E.: Spectral Radiance of the Carbon Arc Between 2500 Å and 1900 Å. Appl. Opt., vol. 10, no. 4, Apr. 1971, pp. 813-818.

18. Hankins, M. A.: The Pyrometric Molarc Radiation Standard at 3800° K. Paper presented at Second Annual Conference of the Temperature Measurements Society (Los Angeles, California), July 17, 1962.

19. Exton, Reginald J.: A Variable Exposure Photographic Pyrometer. ISA Trans., vol. 4, no. 4, Oct. 1965, pp. 365-373.

20. Mihalas, Dimitri: Stellar Atmospheres. W. H. Freeman & Co., c.1970.

21. Snow, Walter L.: Practical Considerations for Abel Inverting of Photographic Data With Application to the Analysis of a 15-kW Wall-Stabilized Arc-Light Source. NASA TN D-6672, 1972.

22. Barr, William L.: Method for Computing the Radial Distribution of Emitters in a Cylindrical Source. J. Opt. Soc. America, vol. 52, no. 8, Aug. 1962, pp. 885-888.

23. Hoel, Paul G.: Introduction to Mathematical Statistics. Fourth ed. John Wiley & Sons, Inc., c:1971.

24. Wiese, W. L.; Smith, M. W.; and Glennon, B. M.: Atomic Transition Probabilities. Volume I - Hydrogen Through Neon. NSRDS-NBS 4, U.S. Dep. Commer., May 20, 1966.

25. Graves, Randolph A.; and Wells, William L.: Preliminary Study of a Wall-Stabilized Constricted Arc. NASA TM X-2700, 1973.

26. Nicolet, W. E.: User's Manual for the Generalized Radiation Transfer Code (RAD/EQUIL). Rep. No. UM-69-9 (Contract NAS1-9399), Aerotherm Corp., Oct. 1, 1969. (Available as NASA CR 116353.)

27. Sutton, Kenneth; Moss, James N.; Falanga, Ralph A.; and Olstad, Walter B.: Outer Planet Entry Probes Aerothermal Environment - Status of Prediction Methodology. AIAA Paper No. 75-1148, Sept. 1975.

28. Nealy, John E.: Absolute Calibration of a Hydrogen Discharge Lamp in the Vacuum Ultraviolet. NASA TM X-3327, 1975.

TABLE I.- SUMMARY OF COMPONENTS OF OPTICAL SYSTEMS

(a) Primary optical system

Spectrometer:
- 1-m vacuum ultraviolet scanning monochromator
- Dispersion, nm/mm:
  - With grating (1) 3.32
  - With grating (2) 1.66
  - With grating (3) 0.83
- Scan rates, nm/min:
  - With grating (2) 0.05, 0.1, 0.2, 0.5, 1, 2, 5, 10, 20, 100, 200
  - With grating (1) . . . . . Twice the values for grating (2)
  - With grating (3) . . . . . One-half the values for grating (2)
- Scan range, nm:
  - With grating (1) 1200
  - With grating (2) 600
  - With grating (3) 300
- Slits:
  - Height, mm . . . . . 20 maximum, 0 minimum
  - Width, mm . . . . . 2 maximum, 0.01 minimum
- Evacuation equipment . . . . . Mechanical and diffusion pumps

Gratings:
- Concave, magnesium-fluoride-coated aluminum reflective surface on borosilicate-crown blank material
- Radius of curvature, mm 955.5
- Grooved area, mm^2 . . . . . 56 × 96

	Grating (1)	Grating (2)	Grating (3)
Grooves/mm	300	600	1200
Blaze angle	13°00'	2°35'	4°8'
Blaze wavelength, nm	1500	150	120

Photomultiplier tubes:
- Two, end on venetian blind

	EMI 9634QR	EMI 9558QAM
Type	S-13 super	S-20
Spectral range, nm	165.0 to 680.0	165.0 to 850.0

Mirror:
- Concave, platinum reflective surface on a 0.953-cm-thick pyrex blank
- Diameter, cm 5.08

Calcium fluoride window:
- Diameter, cm 0.508
- Thickness, cm 0.483

TABLE I.- Concluded

(b) Diagnostic optical system

Spectrometer:
- 1-m modified Czerny-Turner scanning monochromator with collimating mirror and focusing mirror
- Dispersion, nm/mm 0.83
- Effective aperture f/8.7
- Resolution, nm 0.01
- Wavelength range, nm . . . . . 200 to 1300
- Slits:
  - Height, mm . . . . . 20 maximum, 0 minimum
  - Width, mm . . . . . 2 maximum, 0.005 minimum

Grating:
- Plane, magnesium-fluoride-coated aluminum reflective surface on borosilicate-crown blank material
- Ruled area dimensions, mm . . . . . 102 × 102
- Grooves/mm 1200
- Blaze angle . . . . . $17^{\circ}27'$
- Blaze wavelength, nm 500

Film:
- Either 10.2-cm by 12.7-cm spectral analysis plate or Tri-X panchromatic cut film

Quartz window at arc heater:
- Height, mm 23.7
- Width, mm 2.06
- Thickness, mm 2.3

Mirror:
- Plane, reflective front surface in T-arrangement
- Dimensions, cm . . . . . 10.2 × 10.2

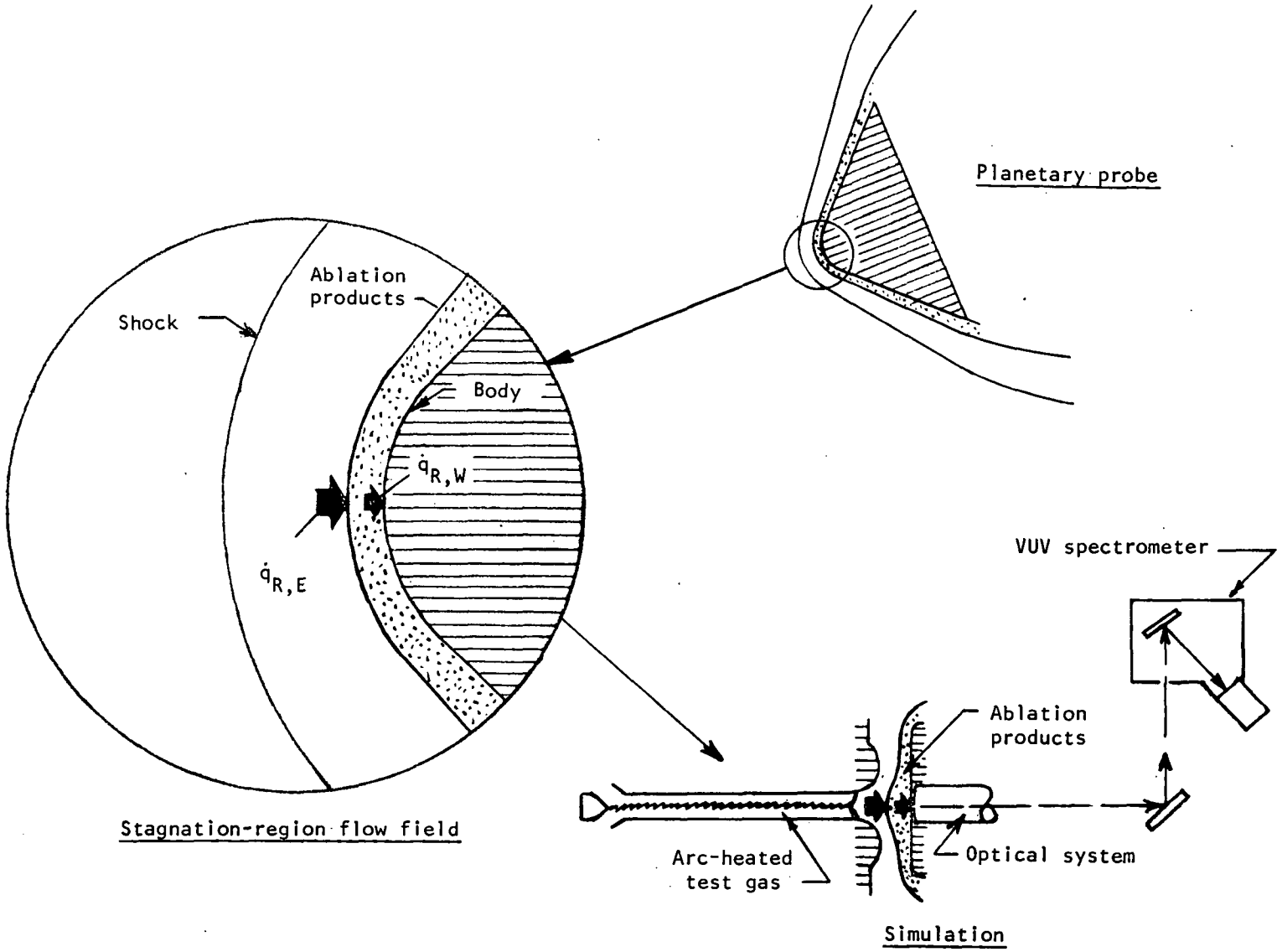

Figure 1.- Concept of laboratory simulation of planetary entry radiating flow field with ablation.

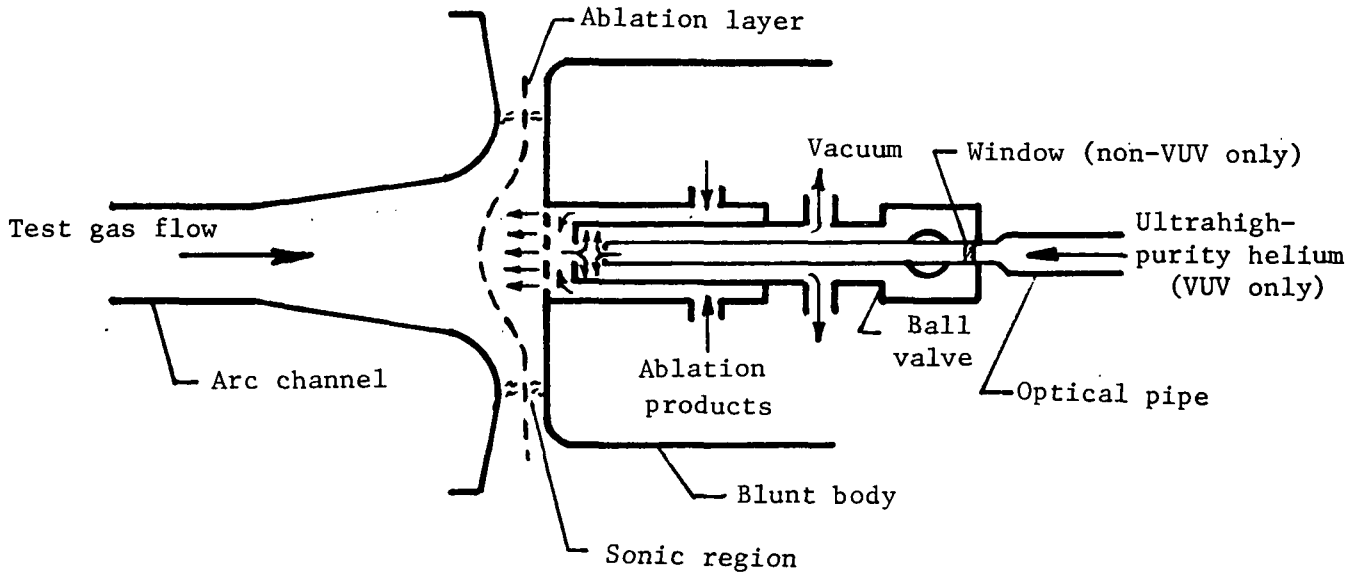

Figure 2.- Schematic of test apparatus in region of simulated ablation gas injection.

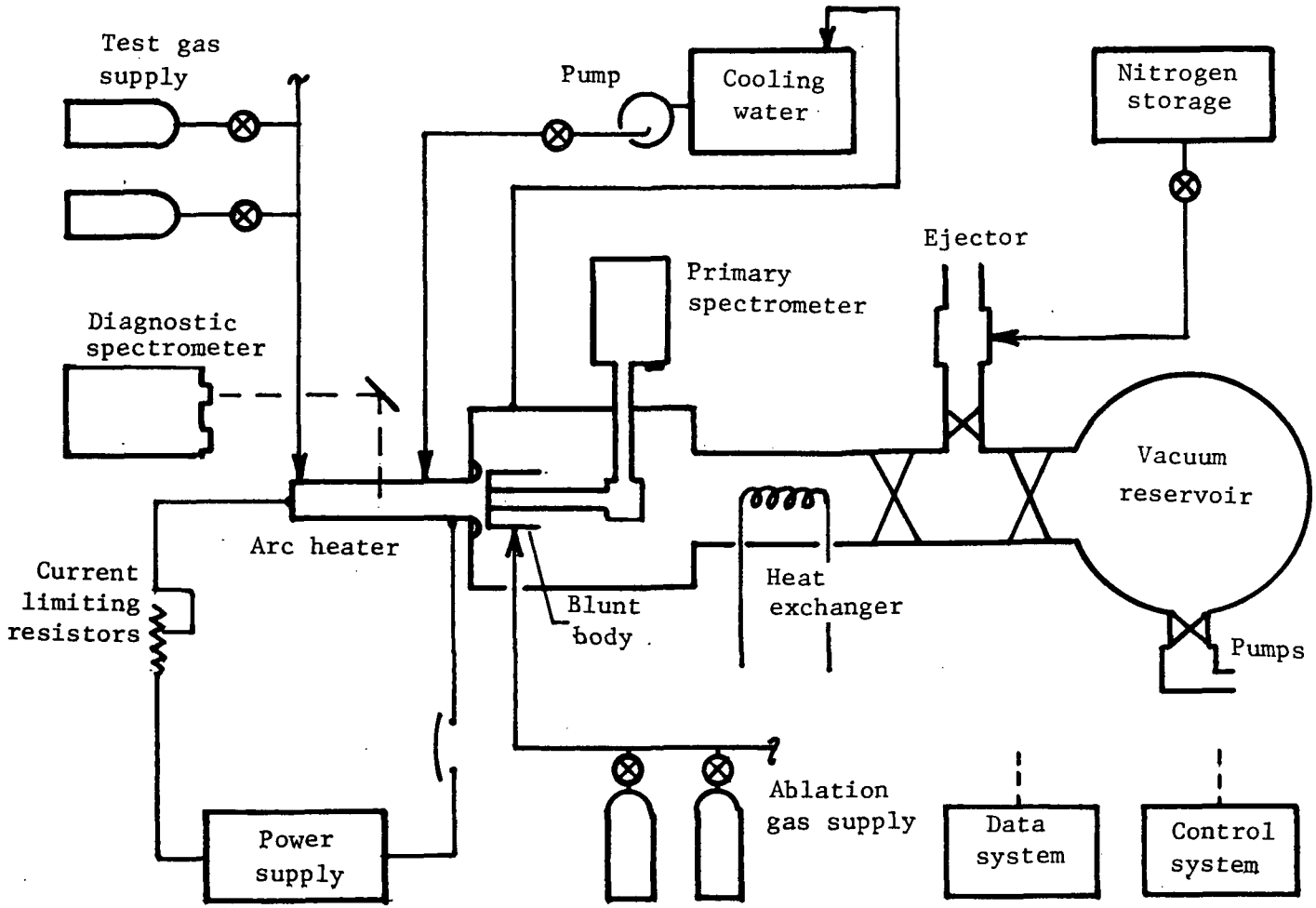

Figure 3.- Schematic view of overall test system.

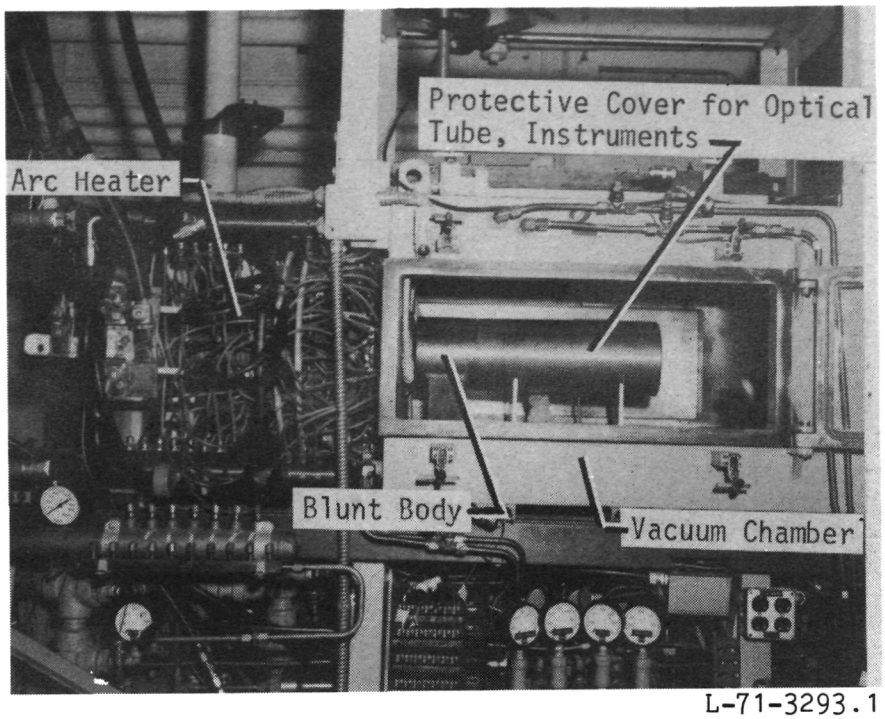

L-71-3293.1

(a) Right side view.

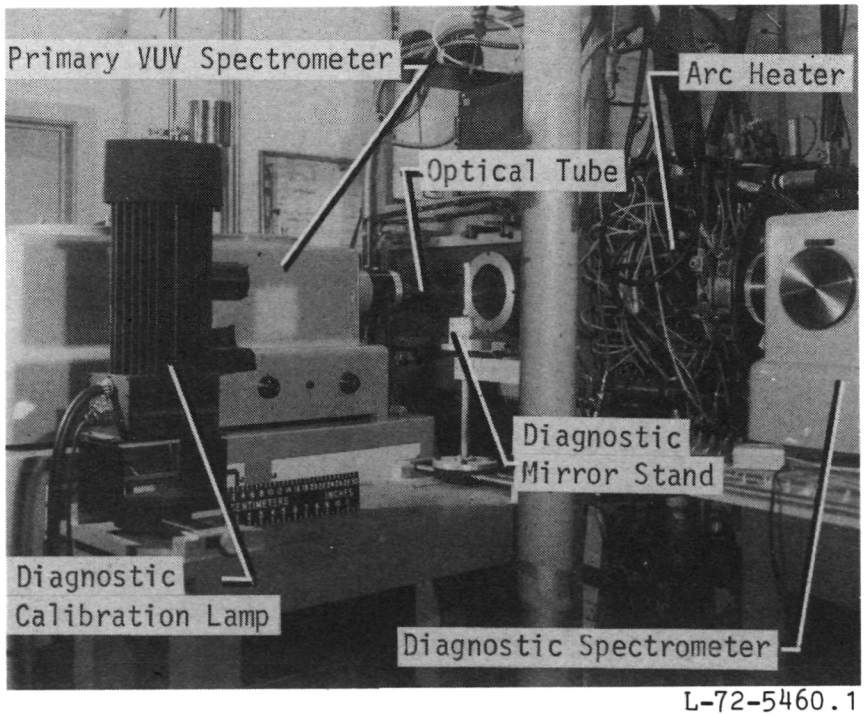

L-72-5460.1

(b) Left side view.

Figure 4.- Photographs of test apparatus.

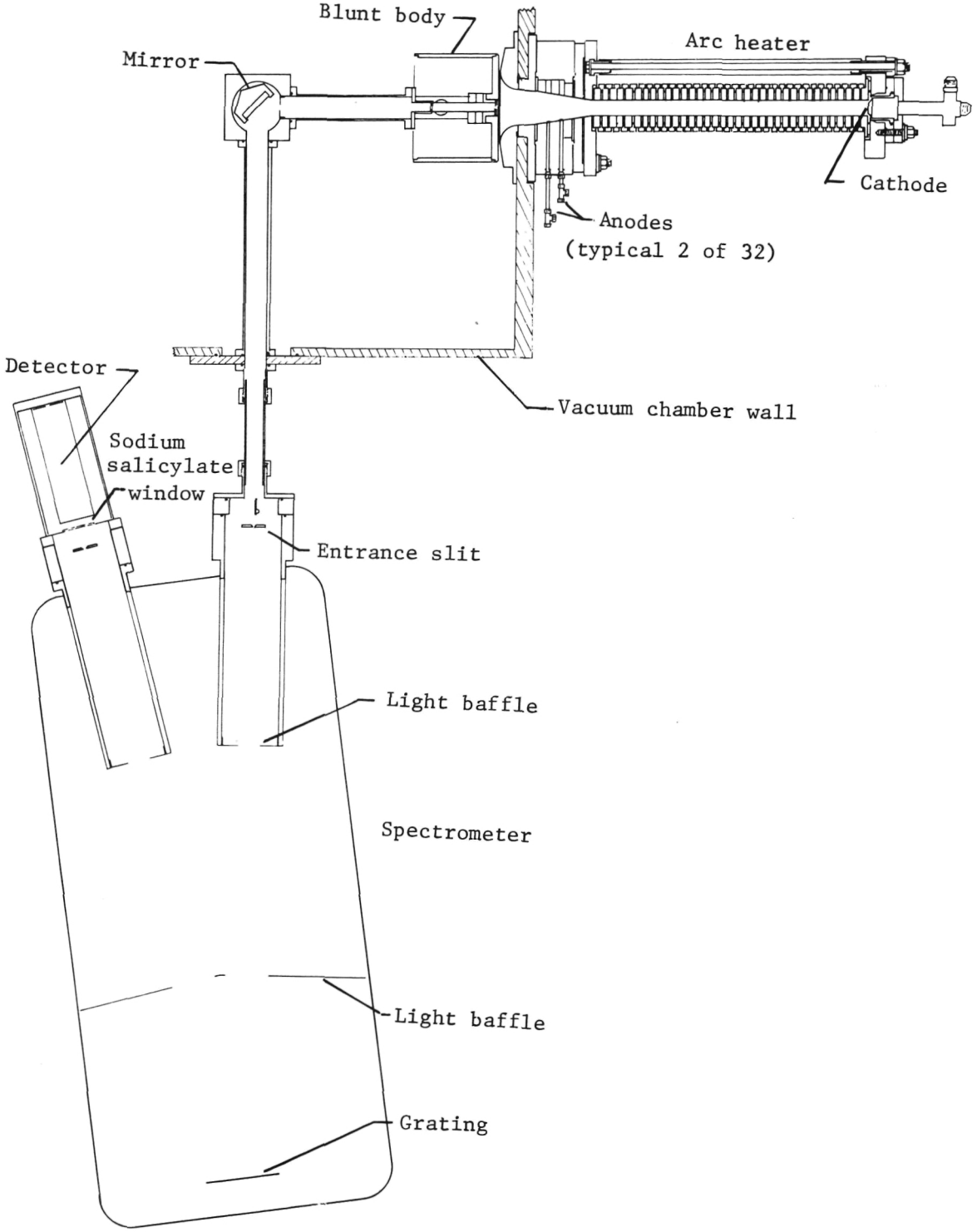

Figure 5.- Scaled drawing of test apparatus including primary optical system.

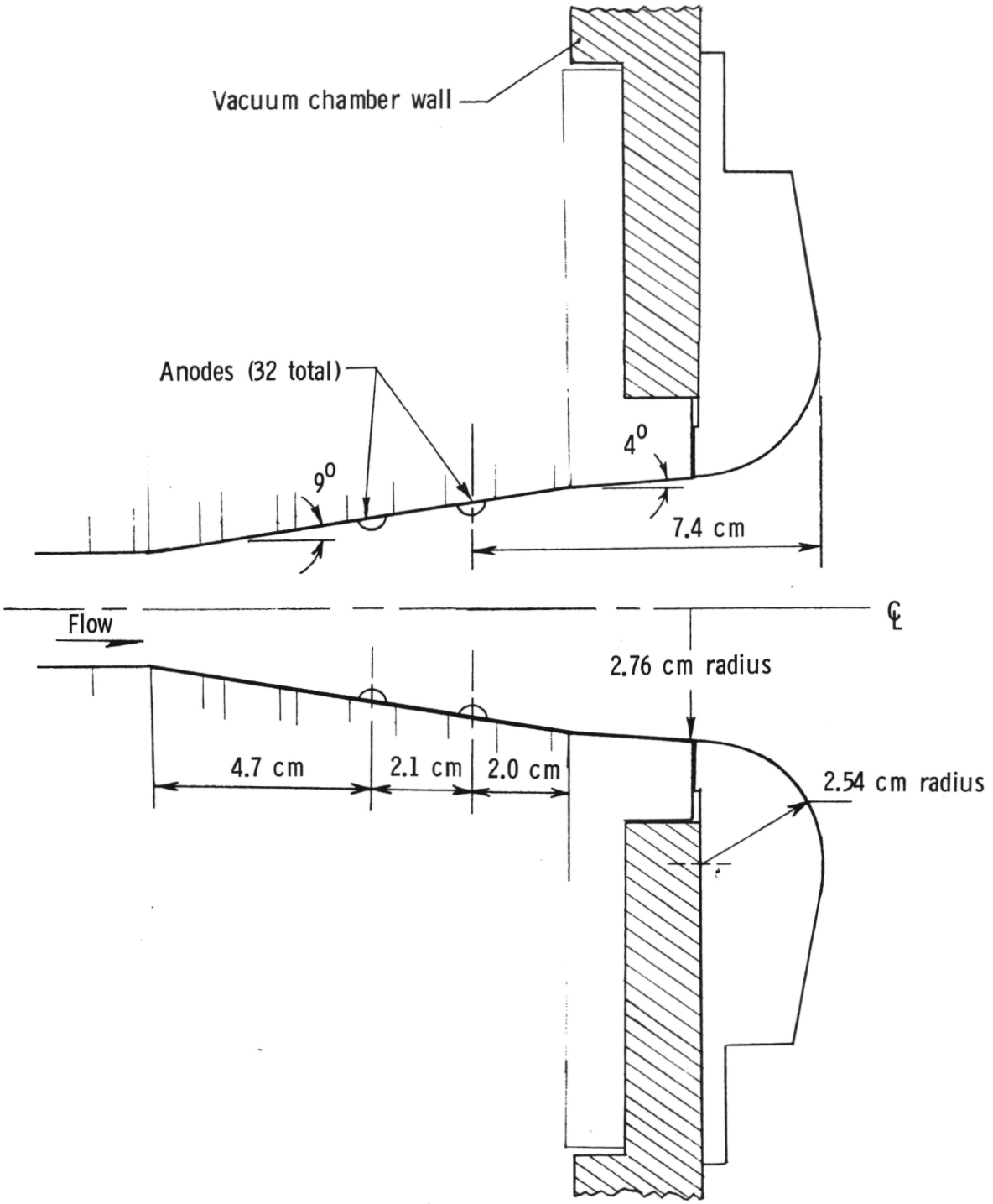

Figure 6.- Arc heater exit region just upstream of blunt body. Geometry is a body of revolution about center line except for anodes.

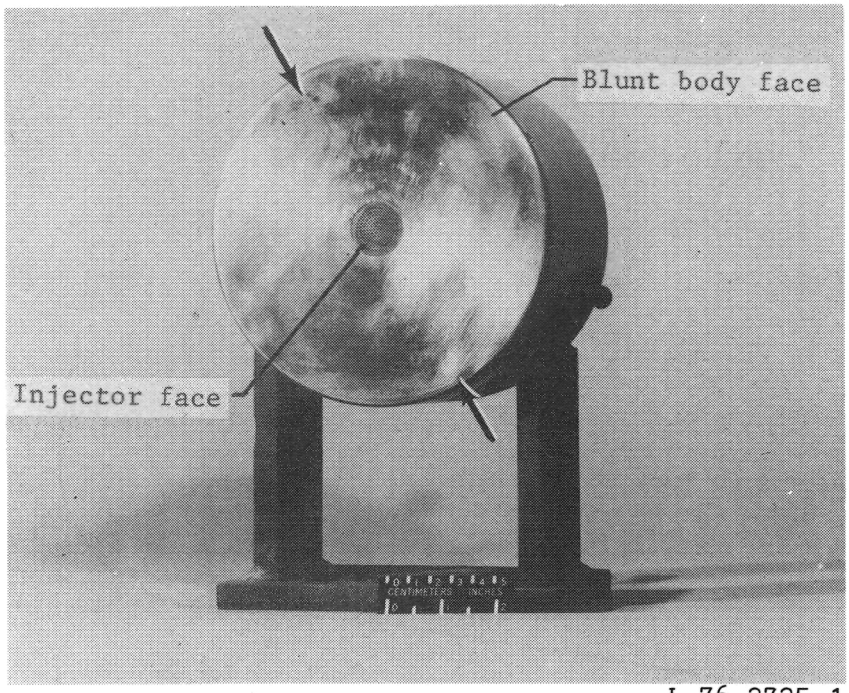

L-76-2725.1

(a) Assembly with injector installed. Note pressure orifices on line between arrows.

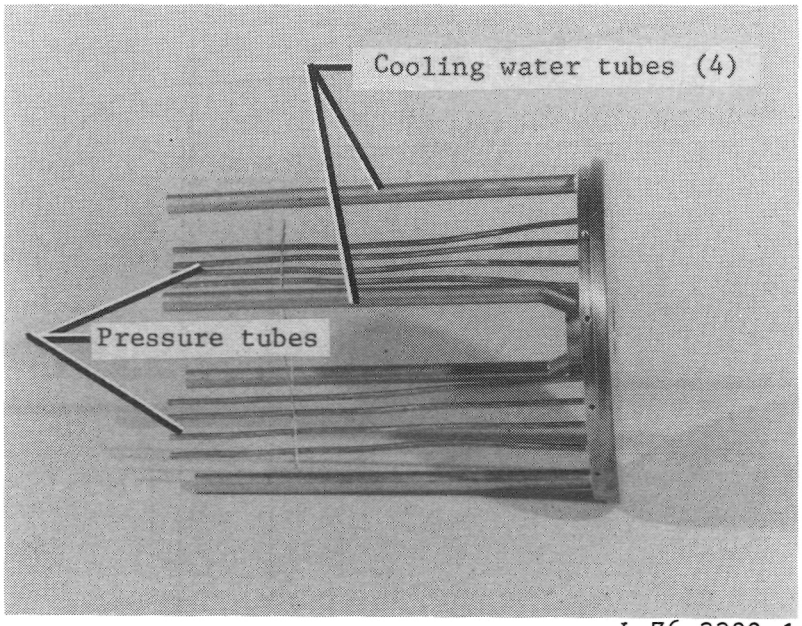

L-76-3300.1

(b) Water-cooled face with pressure tubes exposed.

Figure 7.- Photographs of blunt body.

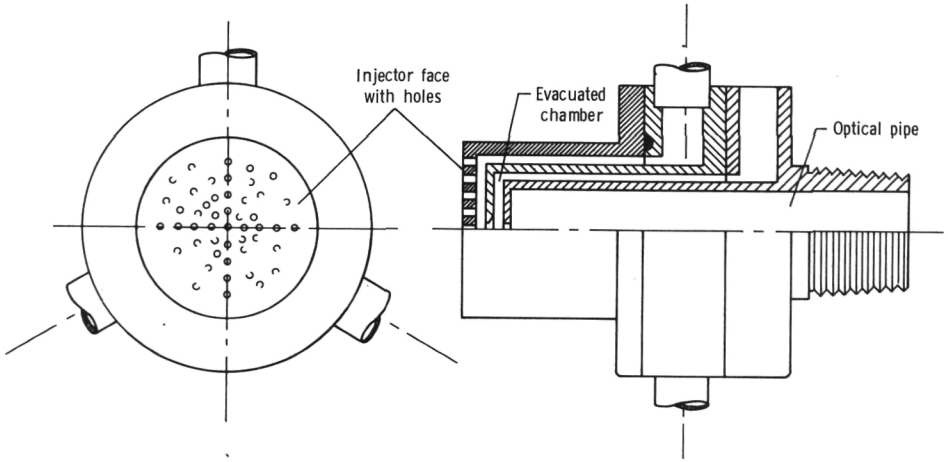

(a) Sketch showing internal passages.

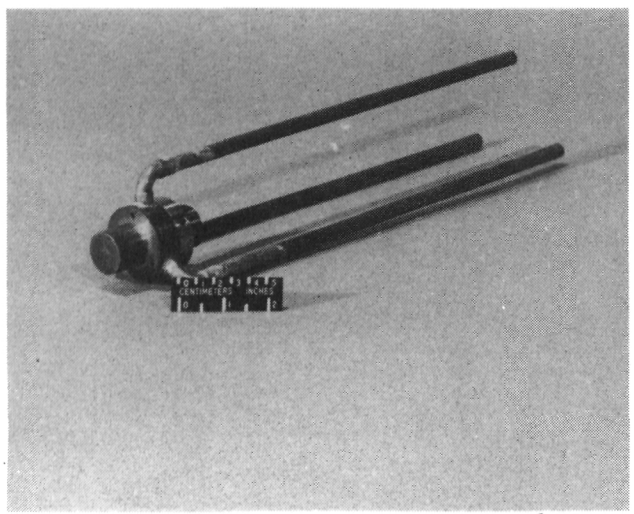

L-76-2727

(b) Assembly.

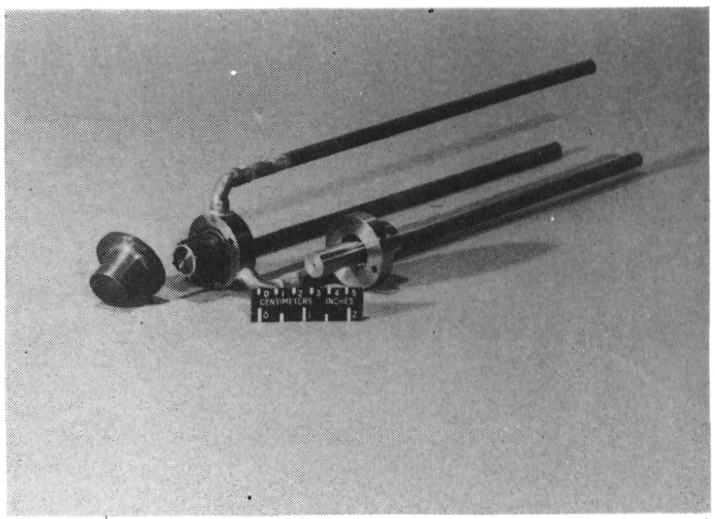

L-76-2726

(c) Parts.

Figure 8.- Simulated ablation gas injector.

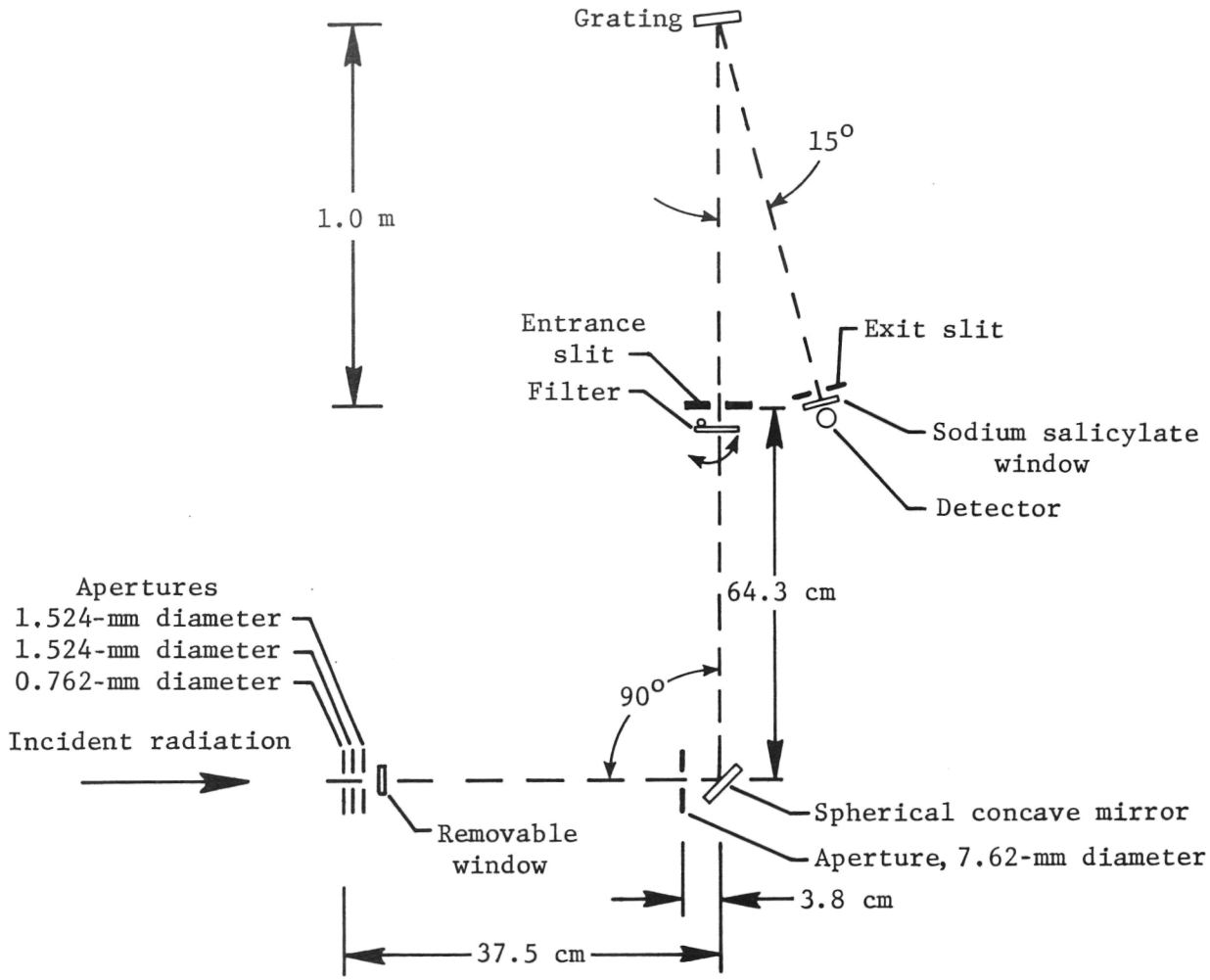

Figure 9.- Primary optical system.

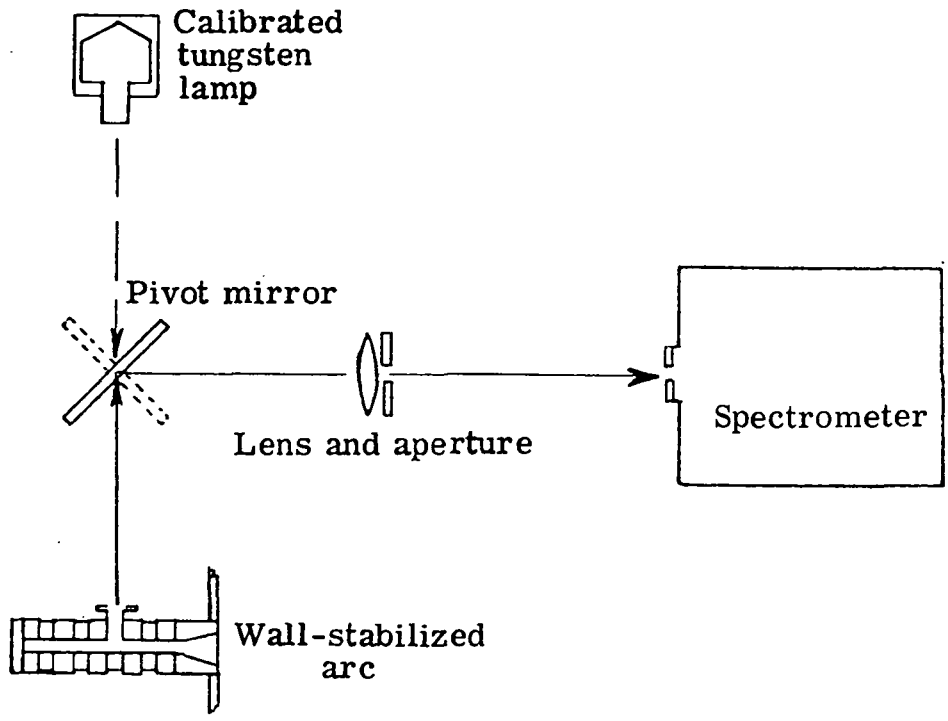

Figure 10.- Diagnostic optical system.

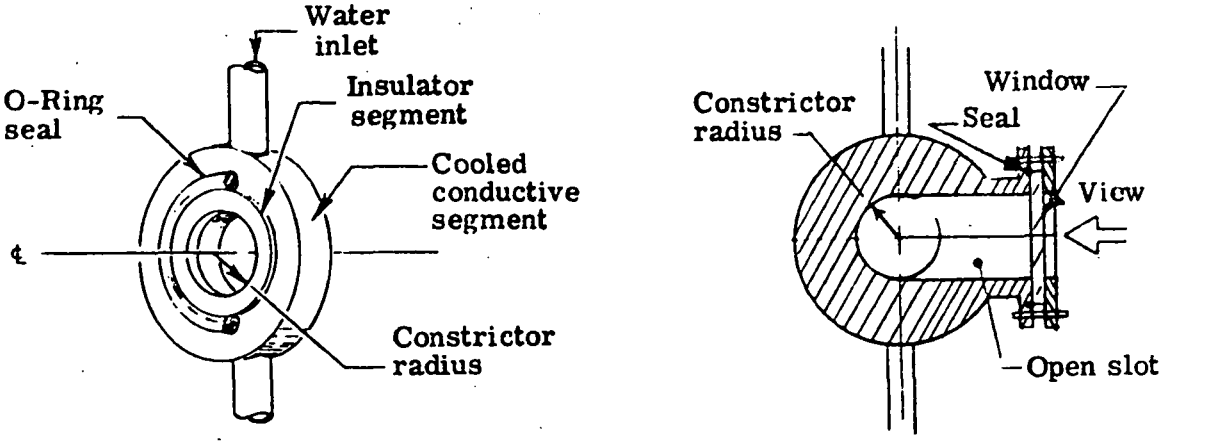

(a) Typical set of segments.

(b) Cross section sketch of special cooled segment with quartz window.

Figure 11.- Arc channel or "constrictor" segments.

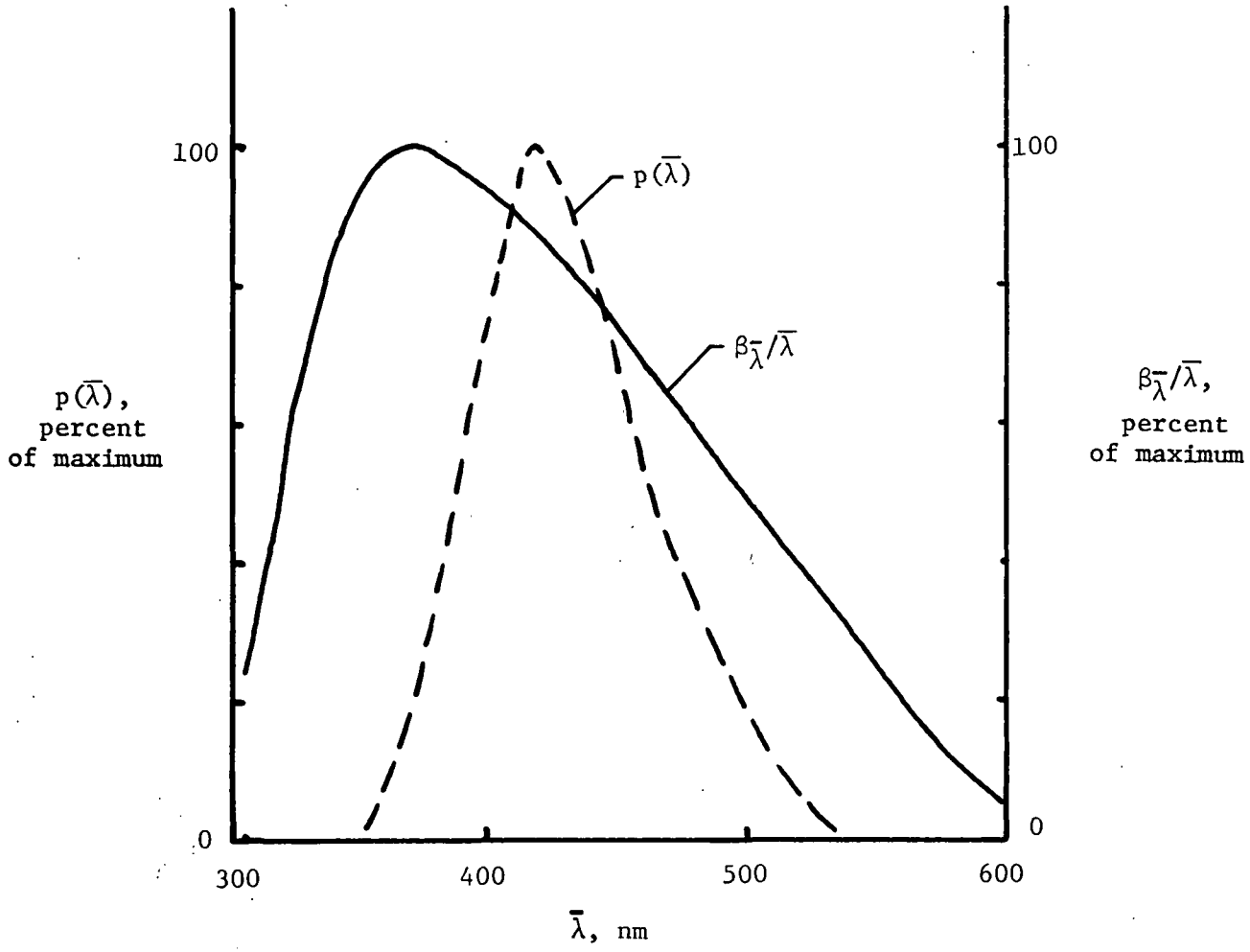

Figure 12.- Relative fluorescent emission probability of sodium salicylate (dashed curve) and relative photomultiplier response divided by wavelength for an S-11 photomultiplier (solid curve).

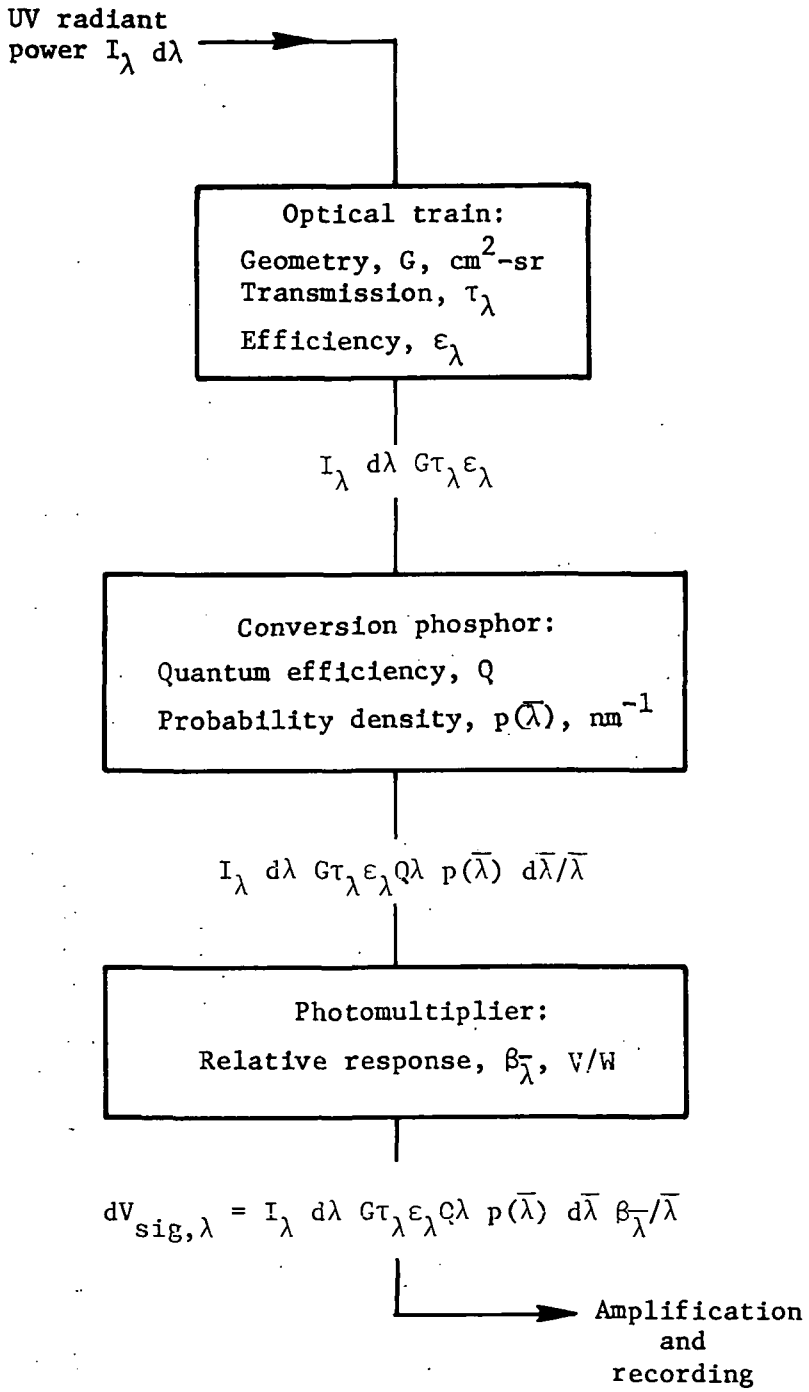

Figure 13.- Flow chart relating the differential output signal corresponding to a differential UV input flux.

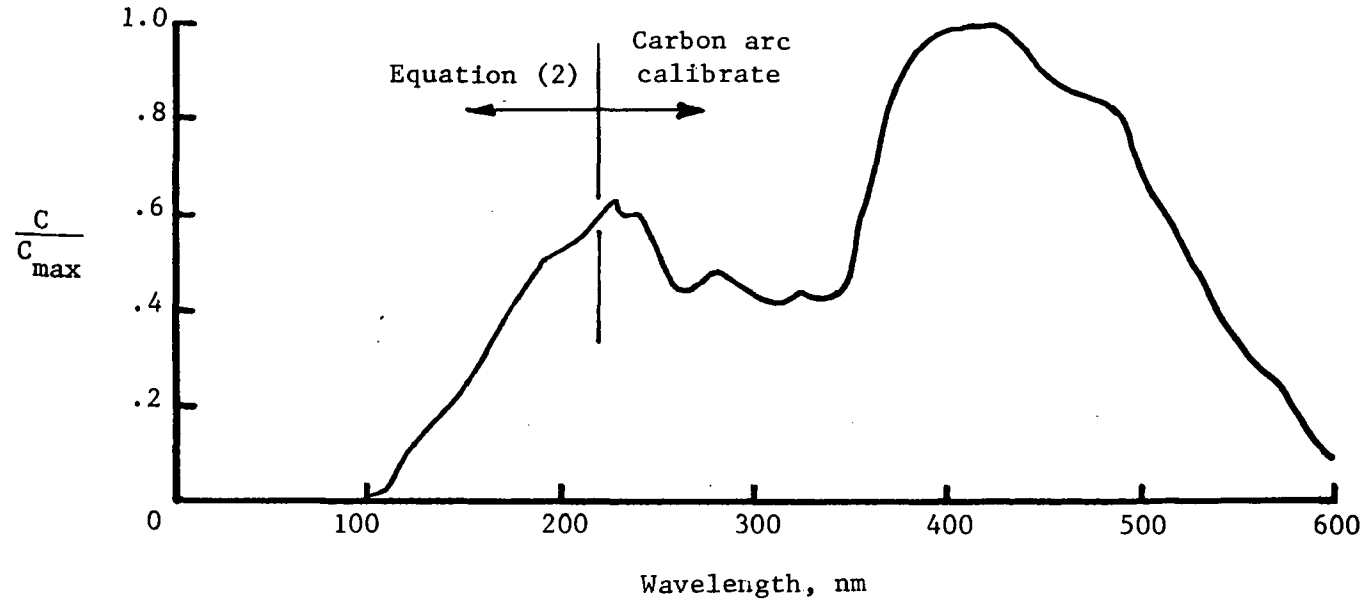

Figure 14.- Relative spectral values of calibration factors used to convert detector signal to intensity. Photomultiplier tube type S-13 super and 600 grooves/mm grating.

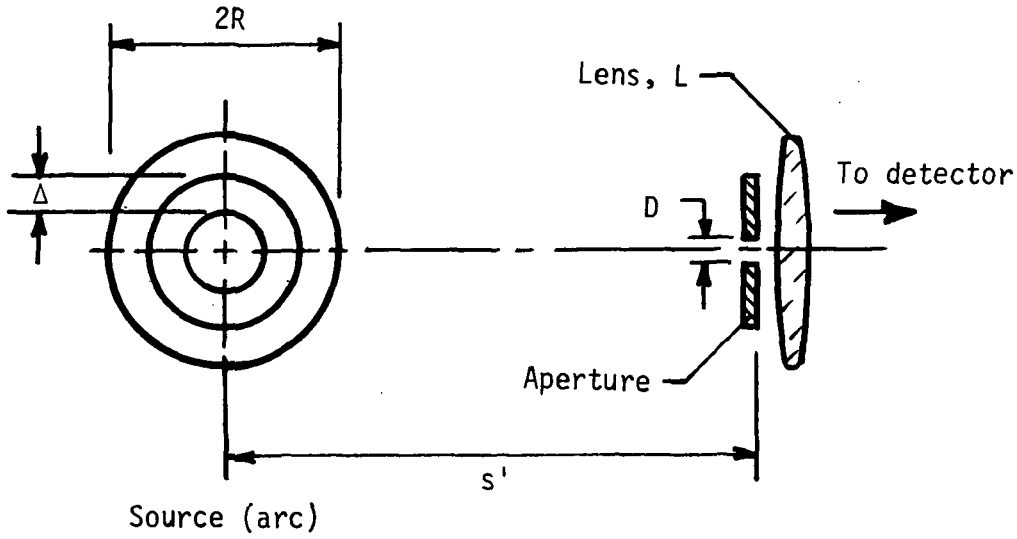

Figure 15.- Model of arc cross section with lens and aperture stop.

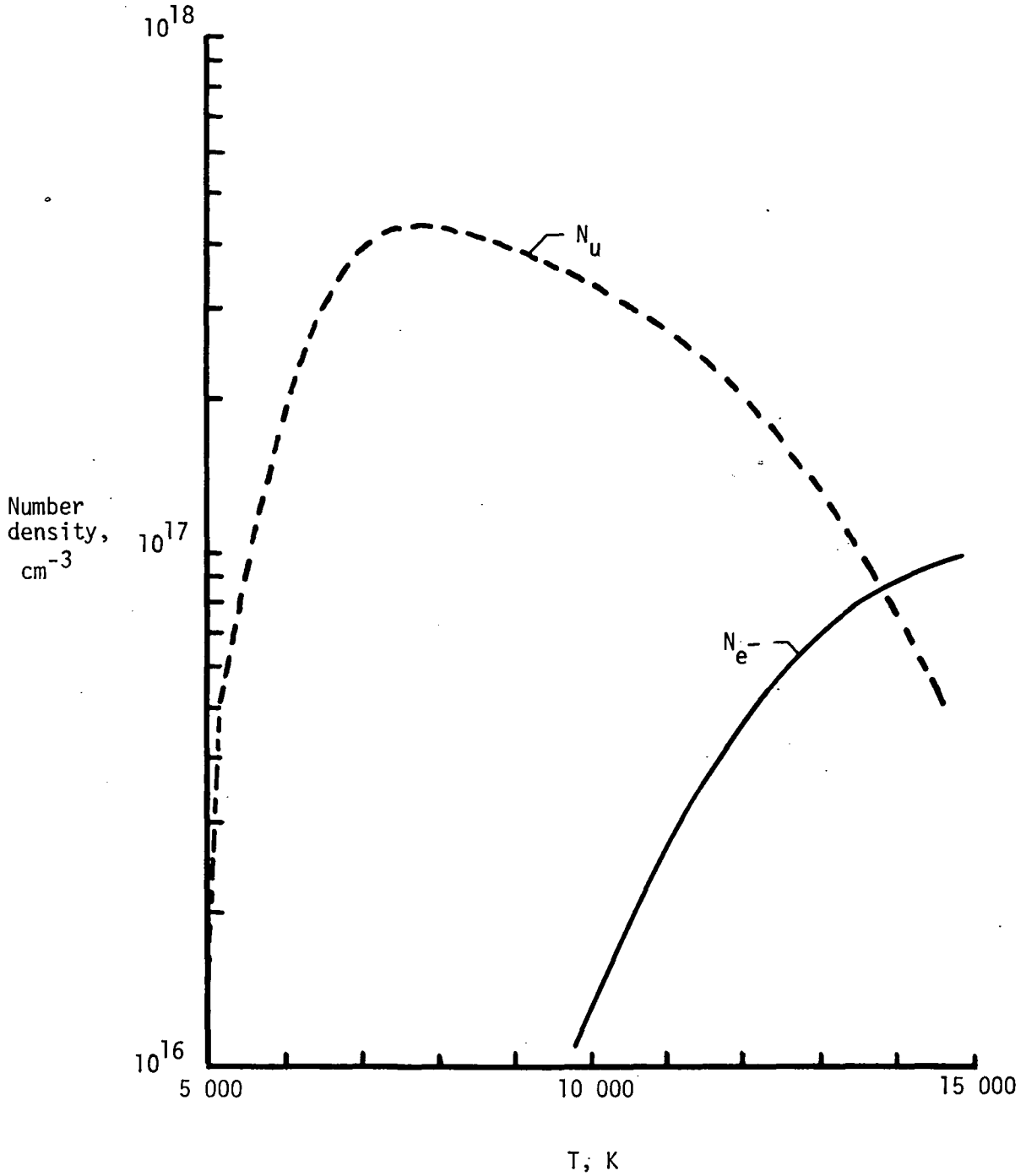

Figure 16.- Electron number density and upper state number density for atomic nitrogen of wavelengths of 493.5 nm and 491.5 nm at pressure of 0.5 atm.

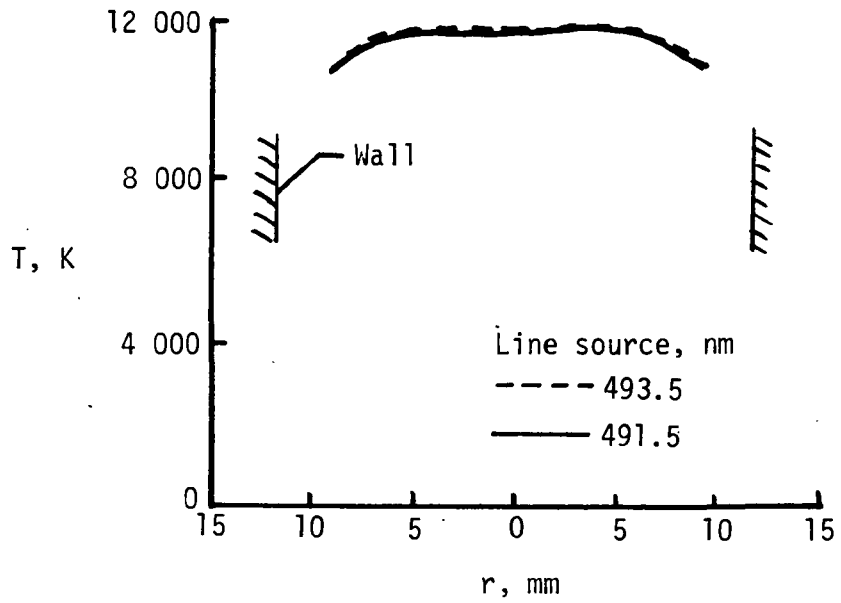

Figure 17.- Radial temperature distribution about midway between cathode and anodes in arc channel. Nitrogen test gas at pressure of 0.5 atm and arc current of 1000 A.

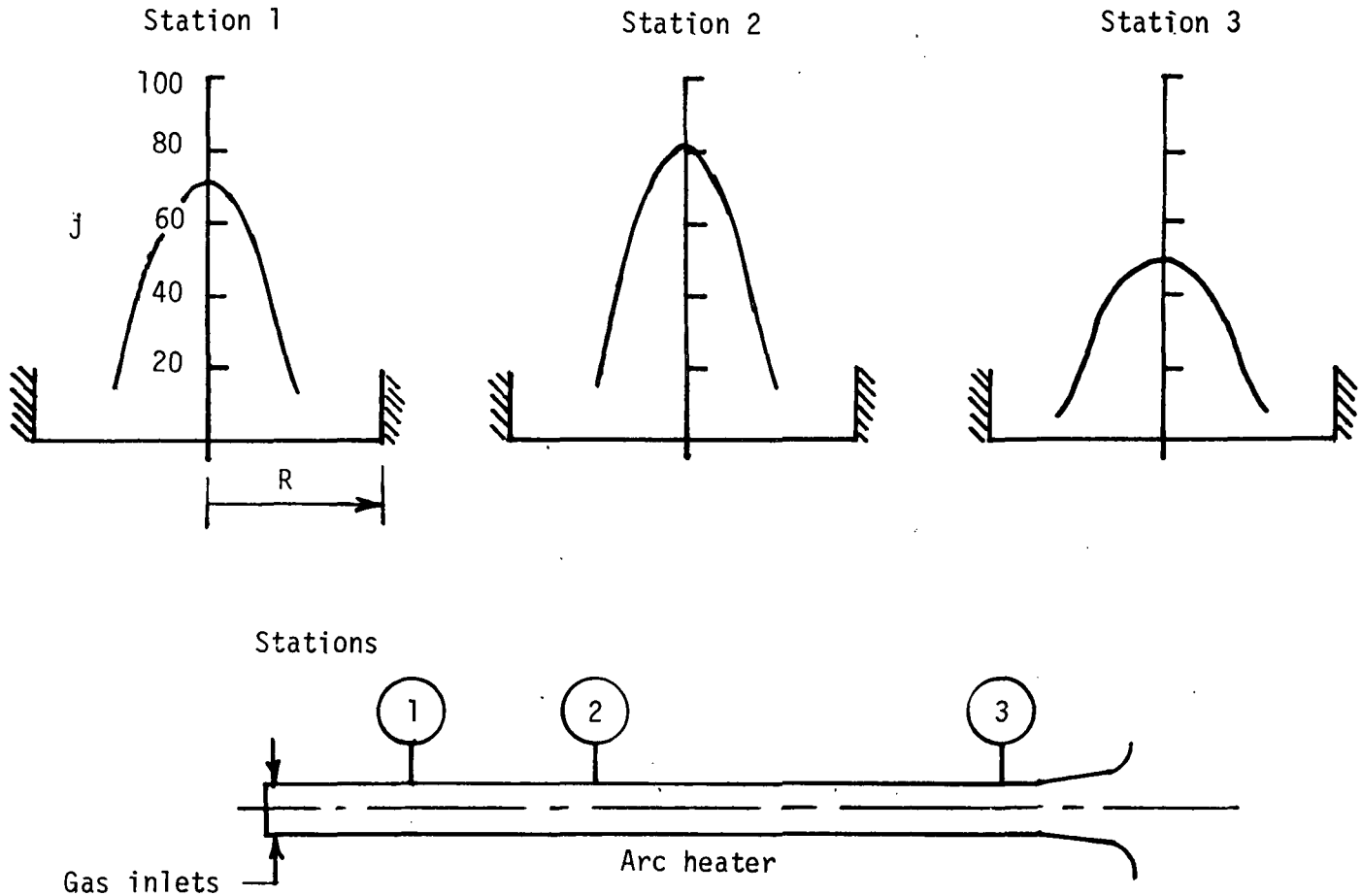

Figure 18.- Radial profile of continuum emission coefficient in apparatus B at wavelength of 495.5 nm for three axial locations. Nitrogen test gas at pressure of 0.5 atm and arc current of about 540 A.

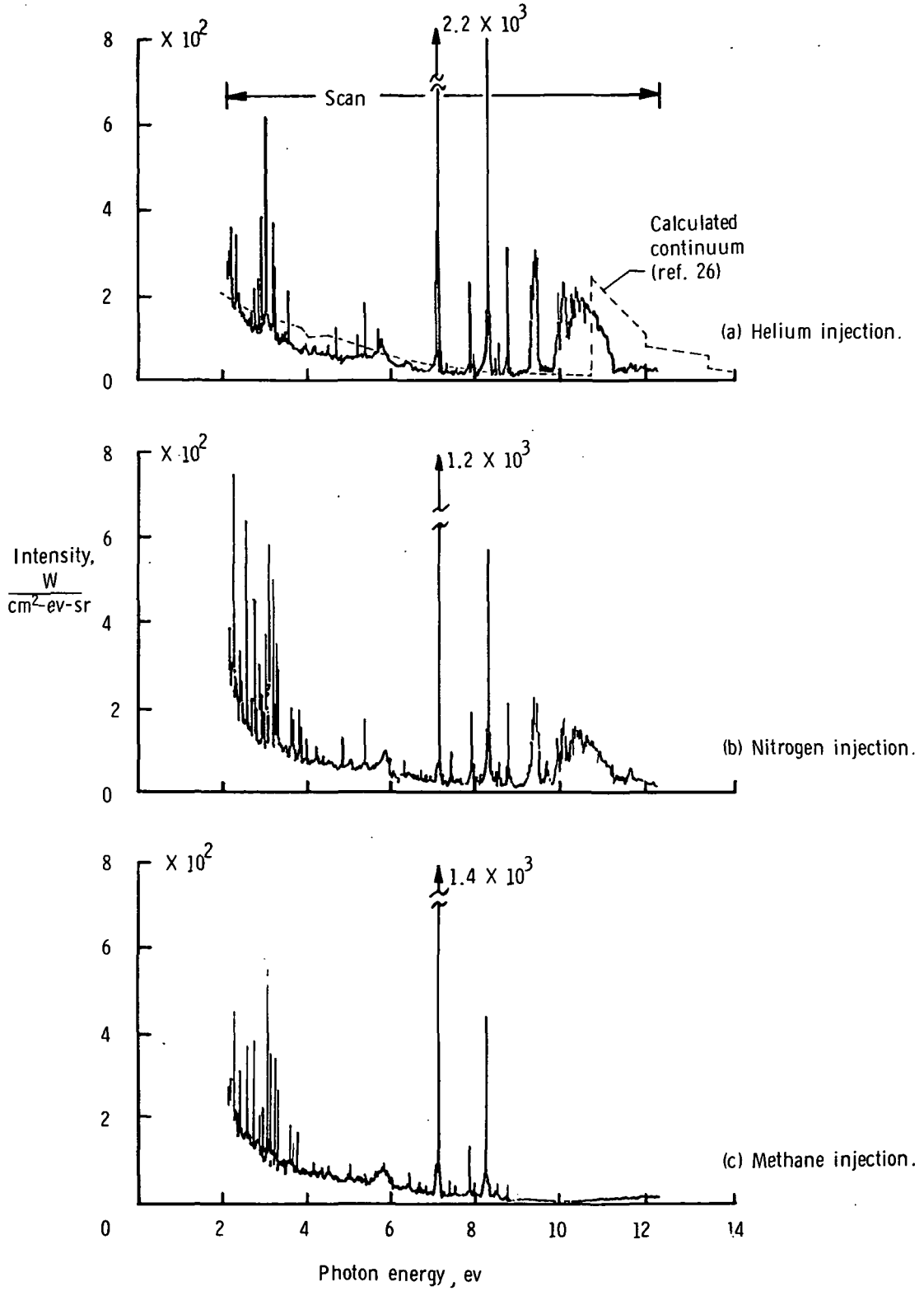

Figure 19.- Measured spectral intensity from radiating nitrogen test gas with different simulated ablation gases injected. Arc current of 1000 A at pressure of 0.5 atm.

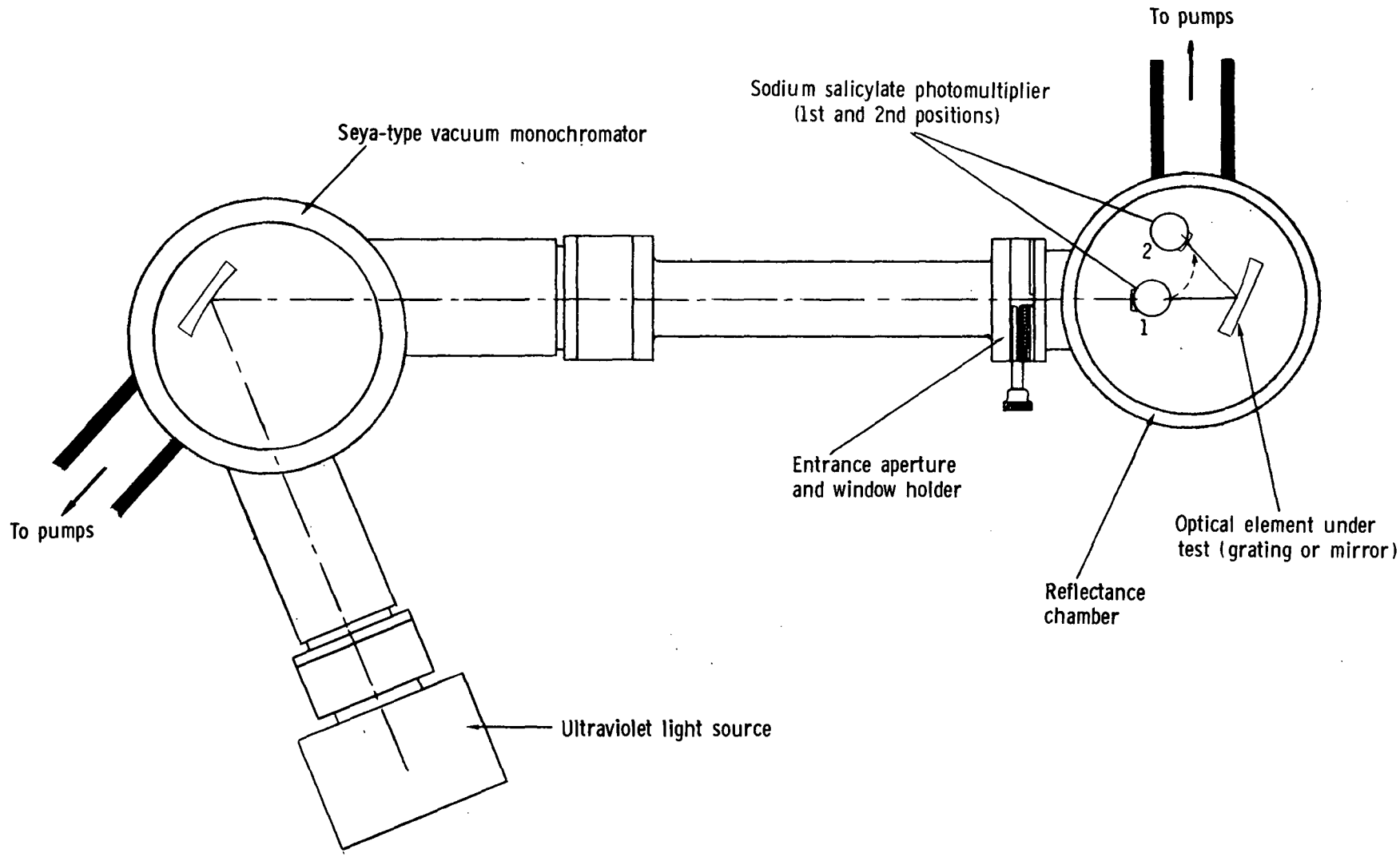

Figure 20.- Apparatus used to determine spectral reflection efficiency of optical elements.

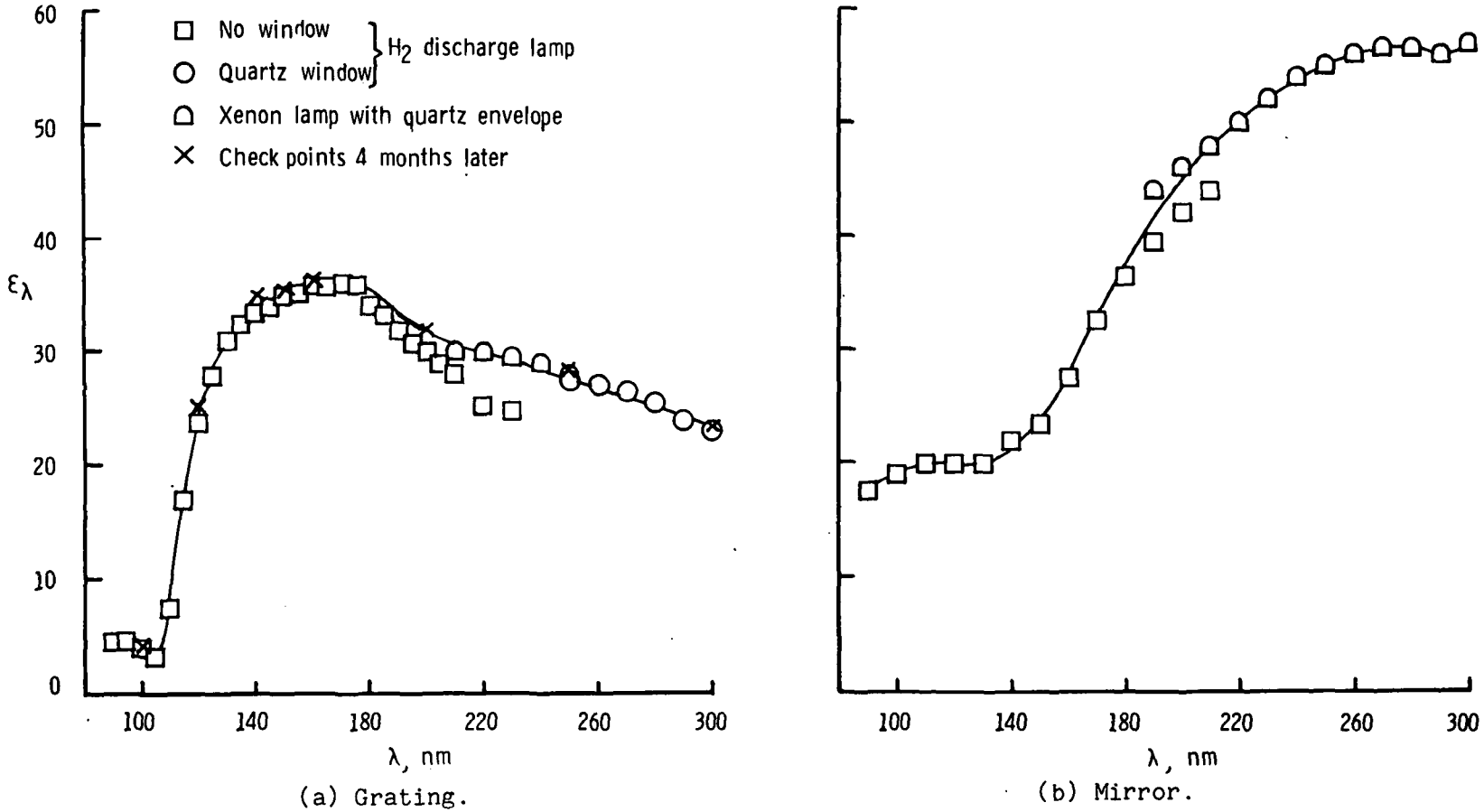

Figure 21.- Measured optical efficiency of mirror and grating.

NATIONAL AERONAUTICS AND SPACE ADMINISTRATION
WASHINGTON, D.C. 20546

OFFICIAL BUSINESS
PENALTY FOR PRIVATE USE $300

SPECIAL FOURTH-CLASS RATE
BOOK

POSTAGE AND FEES PAID
NATIONAL AERONAUTICS AND
SPACE ADMINISTRATION
451

U.S.MAIL

POSTMASTER: If Undeliverable (Section 158 Postal Manual) Do Not Return

"The aeronautical and space activities of the United States shall be conducted so as to contribute . . . to the expansion of human knowledge of phenomena in the atmosphere and space. The Administration shall provide for the widest practicable and appropriate dissemination of information concerning its activities and the results thereof."

—NATIONAL AERONAUTICS AND SPACE ACT OF 1958

NASA SCIENTIFIC AND TECHNICAL PUBLICATIONS

TECHNICAL REPORTS: Scientific and technical information considered important, complete, and a lasting contribution to existing knowledge.

TECHNICAL NOTES: Information less broad in scope but nevertheless of importance as a contribution to existing knowledge.

TECHNICAL MEMORANDUMS: Information receiving limited distribution because of preliminary data, security classification, or other reasons. Also includes conference proceedings with either limited or unlimited distribution.

CONTRACTOR REPORTS: Scientific and technical information generated under a NASA contract or grant and considered an important contribution to existing knowledge.

TECHNICAL TRANSLATIONS: Information published in a foreign language considered to merit NASA distribution in English.

SPECIAL PUBLICATIONS: Information derived from or of value to NASA activities. Publications include final reports of major projects, monographs, data compilations, handbooks, sourcebooks, and special bibliographies.

TECHNOLOGY UTILIZATION PUBLICATIONS: Information on technology used by NASA that may be of particular interest in commercial and other non-aerospace applications. Publications include Tech Briefs, Technology Utilization Reports and Technology Surveys.

Details on the availability of these publications may be obtained from:

SCIENTIFIC AND TECHNICAL INFORMATION OFFICE

NATIONAL AERONAUTICS AND SPACE ADMINISTRATION

Washington, D.C. 20546